



# VCU

Virginia Commonwealth University  
VCU Scholars Compass

---

Theses and Dissertations

Graduate School

---

2016

## COHERENT SPIN TRANSPORT IN NANOWIRE SPIN VALVES AND NOVEL SPINTRONIC DEVICE POSSIBILITIES

Md Iftekhar Hossain  
*Virginia Commonwealth University*

Follow this and additional works at: <https://scholarscompass.vcu.edu/etd>



Part of the [Electrical and Computer Engineering Commons](#)

© The Author

---

Downloaded from

<https://scholarscompass.vcu.edu/etd/4201>

This Thesis is brought to you for free and open access by the Graduate School at VCU Scholars Compass. It has been accepted for inclusion in Theses and Dissertations by an authorized administrator of VCU Scholars Compass. For more information, please contact [libcompass@vcu.edu](mailto:libcompass@vcu.edu).

# COHERENT SPIN TRANSPORT IN NANOWIRE SPIN VALVES AND NOVEL SPINTRONIC DEVICE POSSIBILITIES

A Dissertation submitted in partial fulfillment of the requirements for the degree of Doctor of Philosophy in Electrical and Computer Engineering at Virginia Commonwealth University.

by

Md Iftekhar Hossain

Bachelor of Science in Electrical & Electronic Engineering, BUET, 2011

Director: Supriyo Bandyopadhyay, Ph.D.

Commonwealth Professor, Department of Electrical and Computer Engineering.

Virginia Commonwealth University

Richmond, Virginia

May, 2016.

# Acknowledgement

First of all, I would like to express my deepest gratitude to my PhD supervisor Professor Supriyo Bandyopadhyay. He not only guided me in my research, but his motivation and teaching have completely changed my way of thinking. He gave me plenty of opportunities to become an independent and confident person and achieve leadership qualities. Because of him, besides my research work, I have been privileged to be part of several mentorship programs and also got the opportunity to present my work in several conferences and workshops. Things that I have learnt while working with him will always be a guideline in rest of my life. I would also like to express my sincere appreciation to my co-advisor, Professor Jayasimha Atulasimha for his tireless support, guidance and time. I am also indebted to Professor Arunkumar Subramanian, who is also a collaborator in some of my research projects and one of my committee members, for providing constant support in my research work. I would also like to thank, my committee members, Professor Umit Ozgur, Professor Gary Atkinson and Professor Shiv Khanna, for offering their time, experience and advice to critique my research work.

During the last 4 years, I have received endless support from Dr. Dimitry Pestov, Joshua Starliper, William Paul Clavijo and Dr. Carlos E Castano Londono in terms of training and using the facilities of Nanomaterial Core Characterization Laboratory and Wright Virginia Microelectronic Center. I would like to thank them for making my research journey smoother. Special thanks also go to Mahjabin Maksud and Naveen Kumar Palapati, my fellow graduate students, who were contributors of some of my research projects.

I have to thank my peers, with whom I have been sharing my ideas during dissertation, namely Hasnain Ahmad, Ayan Kumar Biswas, Noel D'Souza, Mohammad Salehi Fashami, Vimal Sampath, Mamun Al-Rashid, Pallabi Sutradhar, Justine Drobitch, Md Ahsanul Abeer, Dhritiman Bhattacharya. I would also like to thank all the staff of the Department of Electrical and Computer Engineering.

Last but not the least, this journey would never have been possible without the encouragement and blessing of my parents, Md Golam Hossain and Farida Sultana, my brother Erfan Mahamud and my wife Tanima Ferdous. I cannot thank them enough for all that they have done for me.

# Table of Contents

<b>Acknowledgement.....</b>	<b>ii</b>
<b>List of Figures .....</b>	<b>vi</b>
<b>Abstract .....</b>	<b>xi</b>
<b>1 Introduction .....</b>	<b>1</b>
1.1 Spin Transport Measurement .....	3
1.1.1 Spin Valve and Inverse Spin Valve .....	3
1.1.2 Hanle Oscillation.....	5
1.2 Spin Relaxation Mechanism .....	7
1.2.1 E-Y Mechanism .....	7
1.2.2 Spin Orbit interaction and D'yakonov Perel' Spin Relaxation Mechanism .....	8
1.3 Magneto-Resistance .....	10
1.4 Organization of The Thesis.....	11
<b>2 Coherent Spin Transport in Nanowire Spin Valves: .....</b>	<b>13</b>
2.1 Experimental Setup:.....	13
2.1.1 Sample Growth and Characterization: .....	13
2.1.2 Measurement Setup:.....	21
2.2 Observing the Spin Valve Effect and The Hanle Oscillation: .....	23
2.3 Spin Relaxation Length in 1D InSb Nanowire .....	28
2.4 Calculation of relative subband populations in the nanowires: Proof that 50-nm diameter nanowires have a single occupied subband.....	31
2.5 Transport model in nanowire spin valve.....	32
2.6 Spin Polarized Current Conduction Mechanism in Space Layer:.....	34
<b>3 Modulation of D'yakonov Perel' mechanism .....</b>	<b>36</b>
3.1 Manipulation of Spin Relaxation with IR Light .....	36
3.2 Experimental Setup.....	39
3.3 IR Sensitivity of Magnetoresistance: .....	40

<b>4</b>	<b>Giant Magneto-conductance due to Magnetic Field Assisted Modulation of Local Electron Concentration: .....</b>	<b>46</b>
4.1	Experimental Setup: .....	52
4.1.1	Sample growth and Characterization: .....	52
4.1.2	Dielectrophoresis: .....	52
4.1.3	Measurement setup: .....	56
4.2	I-V Characteristic With Respect to Magnetic Field:.....	56
<b>5</b>	<b>AMR Sensitivity With Strain.....</b>	<b>59</b>
5.1	Competing Effect of AMR and Spin Valve: .....	60
5.2	Experimental Setup.....	61
5.3	Magnetoresistance measurement with and without IR light .....	61
<b>6</b>	<b>Conclusion:.....</b>	<b>66</b>
	<b>References .....</b>	<b>67</b>
	<b>Curriculum Vitae.....</b>	<b>72</b>

# List of Figures

Figure 1-1: Spin Valve Effect. The magnetoresistance vs magnetic field curve shows two peaks.5

Figure 1-2: Inverse spin valve effect in the presence of localized defects ..... 5

Figure 1-3: Hanle Oscillation. The resistance is oscillating with applied field ..... 6

Figure 1-4: Spin polarizations at different wavevectors in an energy wavevector dispersion relation ..... 7

Figure 2-1 : (a) 100  $\mu\text{m}$  thick rough Al foil. (b) Flat surface after electropolishing. (c) Porous  $\text{Al}_2\text{O}_3$  on top of Al foil. (d) Bottom barrier layer is removed using 5% Phosphoric acid. (e) The pores are filled selectively with Co, InSb and Ni respectively ..... 15

Figure 2-2: Anodization current vs Time behavior during anodization ..... 16

Figure 2-3: (a) Top View of the Alumina ( $\text{Al}_2\text{O}_3$ ) template (b) Cross Sectional View of the Alumina ( $\text{Al}_2\text{O}_3$ ) template (c) Barrier layer at the bottom of the Alumina ( $\text{Al}_2\text{O}_3$ ) (d) Removal of the Barrier layer with 5% Phosphoric Acid ..... 19

Figure 2-4: EDS of spin valve samples..... 20

Figure 2-5:(a),(b) Magnetization curve for Co and Ni using VSM (c) TEM images of a single tri-layer nanowire using bright field imaging ..... 21

Figure 2-6: Experimental setup for magnetoresistance measurement ..... 22

Figure 2-7: The inverse spin valve effect. Room temperature (295 K) longitudinal magnetoresistance plots of three samples showing spin valve troughs. The magnetic field is applied along the axes of the nanowires. The trough positions are indicated with vertical arrows. The horizontal block arrows show the directions in which the field is scanned. The troughs are not symmetric about the resistance axis because of the inevitable asymmetric shapes of the

magnets, which make the coercivities of both cobalt and nickel contacts depend on the field direction. .... 24

Figure 2-8: Scanning electron micrograph of the top surface of a sample where most nanopores have been overfilled, resulting in the nickel spilling out on the surface to form a thin film. The nickel film segregates, forming narrow trenches where the pores are not filled to the brim. Since the nickel contact is essentially a thin film in these samples, its coercivity plummets to ~ 50 Oe since nickel thin films have very low room temperature coercivities of about 20 Oe..... 25

Figure 2-9: Hanle oscillations. Room temperature (295 K) transverse magnetoresistance plots of two samples showing oscillations due to the Hanle effect. The resistance maxima are indicated by arrows and the angle of spin precession is the quantity  $\Phi$ . In sample 1, there is a zero-offset in  $\Phi$  and the maximum closest to zero field is chosen for  $\Phi = 0$ . The block arrow shows the direction of field scan..... 27

Figure 2-10: Hanle Oscillation for three different tilt angle ..... 28

Figure 2-11: Transpot model of an electron in metal semiconductor metal spin valve..... 33

Figure 2-12: Current conduction in a nanowire spin valve..... 34

Figure 3-1: A nanowire spin valve whose two ferromagnetic contacts have opposite signs of tunneling spin polarization..... 36

Figure 3-2 : Spins become randomized due to applied IR illumination. The magnetoresistance peaks also get muted, due to the absence of spin dependent transport. .... 38

Figure 3-3: The magnetizations of the two contacts below and above the threshold magnetic field ..... 40



Figure 3-4: Room-temperature magnetoresistance of a Co-InSb-Ni nanowire spin-valve sample in the dark (above) and under illumination by an infrared lamp radiating in the wavelength range 2-5 $\mu\text{m}$  (below). The zero-field dark resistance was 4.2 ohms..... 41

Figure 3-5: Room-temperature magnetoresistance of another Co-InSb-Ni nanowire spin-valve sample in the dark and under illumination by an infrared lamp radiating in the wavelength range 2-5  $\mu\text{m}$ . The zero-field dark resistance was 9.7 ohms. .... 41

Figure 3-6: Bright field transmission electron micrograph of Co-InSb-Ni nanowire spin valves formed within anodic alumina pores of 50 nm diameter (FM=ferromagnet). The InSb spacer layer length varies from wire to wire because of the fabrication process, but the spread is not large and the average spacer layer length is  $\sim 40$  nm. In the TEM samples, the Co electrodeposition time was intentionally increased to 4 minutes in order to obtain a long Co section for sufficient contrast that will allow unambiguous determination of the InSb spacer layer’s length. In the actual spin valves, the Co section is much shorter because the electrodeposition time was only 30 seconds. .... 43

Figure 4-1: [Color online] (a) An array of Cu wires with a thin oxide coating captured between two Au contact pads. (b) The potential energy diagram in the direction of current flow under an applied bias  $V$ . The Fermi levels in the left and right contacts are denoted by  $E_{FL}$  and  $E_{FR}$ , respectively, while  $q$  is the electron charge. The resistance of the structure can be thought of as being composed of five resistors in series – the resistance  $R_1$  due to the left Au contact, the resistance  $R_2$  due to the left tunnel barrier, the resistance  $R_3$  due to the Cu wire, the resistance  $R_4$  due to the right tunnel barrier and the resistance  $R_5$  due to the right Au contact. The dominant resistances are  $R_2$  and  $R_4$ ..... 47

Figure 4-2 [Color online] (a) When a magnetic field is applied transverse to the direction of current flow, the resulting Lorentz force deflects electrons towards one edge, causing accumulation at one edge (in this case the top edge) and depletion at the opposite edge (in this case the bottom edge). (b) Accumulation shifts the Fermi level upwards with respect to the conduction band edge in a metal while depletion shifts it downwards. Therefore the potential barriers become shorter at the accumulated (top) edge and taller at the depleted (bottom edge). Electrons tunnel through (or thermionically emit over) the barriers much more easily at the top edge than at the bottom edge, making the resistances due to the barriers vastly different at the top and bottom. .... 49

Figure 4-3: (a) 100  $\mu\text{m}$  thick rough Al foil. (b) Flat surface after electropolishing. (c) Porous  $\text{Al}_2\text{O}_3$  on top of Al foil. (d) Bottom barrier layer is removed using 5% Phosphoric acid. (e) Pores are filled with Cu using proper electrolyte and DC electrodeposition. (f) Alumina ( $\text{Al}_2\text{O}_3$ ) layer is removed using Chromic-Phosphoric acid leaving behind free-standing nanorods. .... 53

Figure 4-4: SEM image of free standing Cu nanorods ..... 54

Figure 4-5: EDS spectrum of Cu nanorods on Al substrate, after Alumina is dissolved with hot Chromic/Phosphoric acid..... 54

Figure 4-6: Scanning electron micrograph of two Cu nanowires captured between two Au contact pads..... 55

Figure 4-7: [Color online] (a) Current versus voltage characteristic of a sample plotted for zero and three different magnetic field strengths. (b) Magnetoconductance of the sample (conductance versus magnetic field) at a fixed voltage of 7 V. .... 57

Figure 4-8: [Color online] (a) Current versus voltage characteristics of a sample at zero magnetic field and at two opposite directions of a magnetic field of 39 mT. (b) The same current voltage characteristics plotted in a log-linear scale. ....	58
Figure 5-1: Switching of magnetization in a nanowire spin valve .....	59
Figure 5-2: Cu nanowire between the Co contacts. ....	61
Figure 5-3: Magnetoresistance plot in Spin Valve measurement. ....	62
Figure 5-4: Multiple domains of Co pads where each of them has own favorable magnetic orientation. ....	62
Figure 5-5: Magnetoresistance curve with IR light .....	63
Figure 5-6: MR behavior in IR and without IR light. ....	64
Figure 5-7: Magnetoresistance behavior with respect to the distance of IR light from the sample. ....	65

# Abstract

## COHERENT SPIN TRANSPORT IN NANOWIRE SPIN VALVES AND NOVEL SPINTRONIC DEVICE POSSIBILITIES

A Dissertation submitted in partial fulfillment of the requirements for the degree of Doctor of Philosophy in Electrical and Computer Engineering at Virginia Commonwealth University.

by

Md Iftekhar Hossain

Bachelor of Science in Electrical & Electronic Engineering, BUET, 2011

Director: Supriyo Bandyopadhyay, Ph.D.

Commonwealth Professor, Department of Electrical and Computer Engineering.

Coherent injection, detection and manipulation of spins in semiconductor nanostructures can herald a new genre of information processing devices that are extremely energy-efficient and non-volatile. For them to work reliably, spin coherence must be maintained across the device by suppressing spin relaxation. Suppression can be accomplished by structural engineering, such as by confining spin carriers to the lowest subband in a semiconductor quantum wire. Accordingly, we have fabricated 50-nm diameter InSb nanowire spin valves capped with Co and Ni nanocontacts in which a single conduction subband is occupied by electrons at room temperature. This extreme quantum confinement has led to a 10-fold increase in the spin relaxation time due to dramatic suppression of the D'yakonov -Perel' (DP) spin relaxation mechanism. We have observed the spin-valve and Hanle effects at room temperature in these systems. Observing both effects allowed us to estimate the carrier mobility and the spin relaxation length/time and we found that the latter is ~10 times larger than the value

reported in bulk InSb despite a four orders of magnitude decrease in the carrier mobility due to surface roughness scattering. We ascribe this dramatic increase in spin relaxation time to the suppression of the DP relaxation mode due to single subband occupancy.

Modulation of spin relaxation rate by an external agent can open new possibilities for spintronic devices. Any agent that can excite electrons from the lowest subband to higher subbands will dramatically increase the DP spin relaxation rate. We have shown that the spin relaxation rate in InSb nanowires can be modulated with infrared light. In the dark, almost all the electrons in the nanowires are in the lowest conduction subband, resulting in near-complete absence of DP relaxation and long spin coherence length. This results in a high resistance state in a spin valve whose ferromagnetic contacts have anti-parallel spin polarizations. Under infrared illumination, higher subbands get populated and the DP spin relaxation mechanism is revived, leading to a three-fold decrease in the spin relaxation length. As a result, injected spins flip in the spacer layer of the spin valve and this causes the spin valve resistance to drop. Therefore, this effect can be exploited to implement an infrared detector.

We also studied the transport behavior of a single nanowire (~50 nm diameter) captured between two non-magnetic contact pads. The wire was attached between the pads using dielectrophoresis. A giant (~10,000,000%) negative magnetoresistance at 39 mT field was observed at room temperature in Cu nanowires contacted with Au contact pads. In these nanowires, potential barriers form at the two Cu/Au interfaces because of Cu oxidation that results in an ultrathin copper oxide layer forming between Cu and Au. Current flows when electrons tunnel through, and/or thermionically emit over these barriers. A magnetic field applied transverse to the direction of current flow along the wire deflects electrons toward one edge of the wire because of the Lorentz force, causing electron accumulation at that edge and depletion at the other. This

makes the potential barrier at the accumulated edge shorter and at the depleted edge taller. The modulation of the potential barrier height with a magnetic field dramatically alters the tunneling and/or thermionic emission rate causing a giant magnetoresistance.

Currently, effort is underway to demonstrate strain sensitive anisotropic magnetoresistance (AMR) in a single Co-Cu-Co nanowire spin valve. AMR is caused by spin-orbit coupling effects which makes the resistance of a ferromagnet depend on the angle between the direction of current flow and the magnetization. The resistance maximizes when the angle is  $0^\circ$  or  $180^\circ$  and minimizes when the angle is  $90^\circ$ . When an external magnetic field is applied in a direction opposite to a ferromagnet's magnetization, the latter begins to rotate in the direction of the field and hence its resistance continuously changes. This results in a trough in the magnetoresistance of a spin valve structure between the two fields when the magnetization starts to rotate and when the magnetization completes the rotation. We have observed a magnetoresistance peak (instead of trough) in the Co-Cu-Co spin valve, which is due to the normal spin valve effect that overshadows AMR. However, when an intense infrared light source is brought close to the sample, the peak gets overshadowed by a trough, showing that the AMR effect becomes dominant. We attribute this intriguing feature to the fact that the AMR effect is strongly influenced by strain. Heating by the light source generates strain in the Co contacts owing to unequal thermal expansion of Co and the underlying substrate. We also observed that the AMR effect becomes more pronounced as the light source is brought closer to the sample, resulting in increased heating and hence increased strain generation.

# 1 INTRODUCTION

---

Conventional electronic devices are based on the transport of electric charge carriers – electrons and holes – in semiconductors such as silicon [1]. There is currently a drive to exploit the 'spin' of the electron rather than its charge to create a new generation of 'spintronic' devices which will be more versatile and energy-efficient than charge based devices. Adding the spin degree of freedom provides new effects, new capabilities and new functionalities. A watershed event in spintronics was the proposal for the Datta-Das Spin Field Effect Transistor which is similar to the conventional MOSFET, except the current flowing between the ferromagnetic source and drain contacts is modulated with a gate potential that does not alter the charge carrier concentration in the channel, but precesses the spin polarization of the carriers. This precession is done via modulation of the Rashba spin-orbit interaction caused by the electric field due to the gate potential. Therefore, in principle, the energy dissipation  $\Delta Q \Delta V$  associated with changing the charge concentration in the channel of the transistor ( $\Delta Q$  = change in channel charge and  $\Delta V$  = change in voltage needed to change the charge in the device by the amount  $\Delta Q$  ) is mostly absent. However, there are serious roadblocks encountered by the Datta-Das transistor. First, changing the spin polarization of the carriers will cause the source to drain current to vary if and only if the source acts as an efficient spin injector (or polarizer) and the drain acts as an efficient spin filter (or analyzer). Second, the spin polarization in the channel should not be randomized by spin relaxation events. Third, the channel should be one-dimensional; otherwise, ensemble averaging over the transverse wavevector components of the electrons randomizes the spin precession and dilutes the gate modulation of the source to drain current (transistor action).

In this study, the second and third issues are addressed. The motivation of this work is to study spin transport in a one dimensional semiconductor channel and seek ways to suppress rapid spin relaxation. Spin transport is studied in a one-dimensional InSb spin valve structure which has two ferromagnetic contacts sandwiching a 50-nm diameter InSb wire at room temperature. InSb was the material of choice in this study since it is a narrow gap semiconductor with strong Rashba spin orbit interaction, which is easily gate-tunable in the Datta-Das type spin transistor. It is, in fact, the ideal material for the Datta-Das transistor, except that the strong Rashba interaction also causes strong DP relaxation. Therefore, successful suppression of the DP mechanism in an InSb structure will be a remarkable advance; it will result in an ideal channel material for the Datta-Das transistor since it has strong Rashba interaction and yet weak spin relaxation.

The samples (Co-InSb-Ni nanowire spin valves) were grown with porous Alumina ( $\text{Al}_2\text{O}_3$ ) template [2]–[4]. The spin valve effect and the Hanle effect were observed in these samples at room temperature, indicating successful spin injection, filtering and somewhat coherent spin transport. We have found that in a 1-D quantum wire, the spin relaxation time increases by 10 times over that in bulk or quantum well. All these facts bode well for the Datta-Das transistor. We were also able to use infrared (IR) light to modulate the spin relaxation rate in the nanowires, thereby opening the door to a novel spintronic IR detector.

In our experiments, we measured spin transport through  $\sim 10^8$  wires in parallel since the sample fabrication technique was based entirely on electrochemical self-assembly and no patterning/lithography was involved. Consequently, the spin transport parameters were ensemble averaged over nearly a hundred million nanowires. While such experiments still shed light on important features such as suppression of spin relaxation by one-dimensional confinement, they



do not yield unambiguous quantitative values for spin relaxation time or length in a single nanowire. Our next goal was to study spin transport in a single nanowire. For that, we have patterned Cobalt electrodes on a silicon substrate with electron beam lithography, released the nanowires from the Alumina templates and placed a single nanowire between the Cobalt pads using dielectrophoresis. We have found that such structures exhibit a plethora of interesting behavior driven by complex physics.

## **1.1 SPIN TRANSPORT MEASUREMENT**

Two well-known phenomena which demonstrate coherent spin transport are the “spin valve effect” and the “Hanle conductance oscillation”. In the former effect, the magnetoresistance of a tri-layered structure, consisting of a paramagnet interposed between two ferromagnets that inject and detect spins, exhibit either a peak or a trough between the coercive fields of the two ferromagnets. In the latter effect, the conductance of the structure exhibits periodic oscillation in a magnetic field that is non-collinear with the magnetization of two ferromagnets. In the following two subsections, we discuss them.

### **1.1.1 Spin Valve and Inverse Spin Valve**

The spin valve device is a tri-layered structure consisting of two ferromagnetic contacts and a semiconductor spacer. One contact acts like a spin polarizer and injects spin-polarized electrons into the spacer. The other contact is a spin analyzer that transmits electrons depending on their spin polarization. The resistance of the spin valve is highest when the two contacts have anti-parallel magnetization and lowest when they have parallel magnetization (figure 1-1).

In the “spin valve” experiment, a strong magnetic field is first applied (+H in figure 1-1) in the direction of current flow so that both the ferromagnetic contacts are polarized in the same direction along the field. Then, the magnetic field is reduced to zero, but the ferromagnetic contacts hold their magnetic alignment because of their remnant magnetization. Next, the magnetic field direction is reversed (-H according to figure 1-1) and the field strength is increased gradually. Since one ferromagnetic contact will have lower coercivity than the other, it will respond to the field first and flip its magnetization so that we will have an antiparallel configuration of the contacts like the one in figure 1-1. Hence the spin valve’s resistance will go high since the spins injected by one contact will be blocked by the other. If we continue to increase the field strength and exceed the other contact’s coercivity as well, then that too will flip its polarization, placing both contacts in the parallel configuration again and the resistance will drop. Therefore, the magnetoresistance will exhibit a peak between the coercive fields of the two contacts. This is the “spin-valve” effect.

A peculiarity arises if the spacer layer has one or more defects close to one contact. If the energy levels of the defect states are resonant with the energy of the electrons, then the electrons will resonantly tunnel through the defect energy level and this can reverse the spin polarization of the contact near the defects. In that case, the contacts will have parallel magnetization only between their coercive fields and anti-parallel magnetization at any other field strength. [5] As a result, we will see a trough instead of a peak in the magnetoresistance occurring between the coercive fields of the two contacts (figure 1-2). This is referred to as the inverse spin valve effect. Since the trap formation is random, clearly some samples will exhibit the normal spin valve effect and show a peak, while others will exhibit the inverse effect and show a trough.

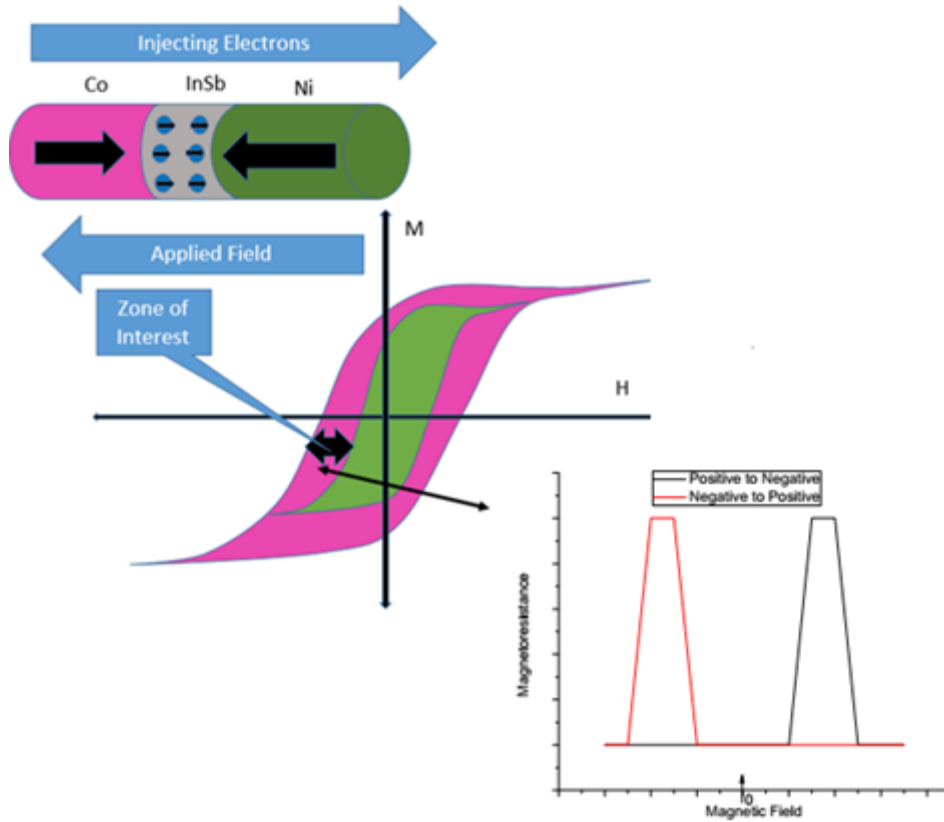


Figure 1-1: Spin Valve Effect. The magnetoresistance vs magnetic field curve shows two peaks.

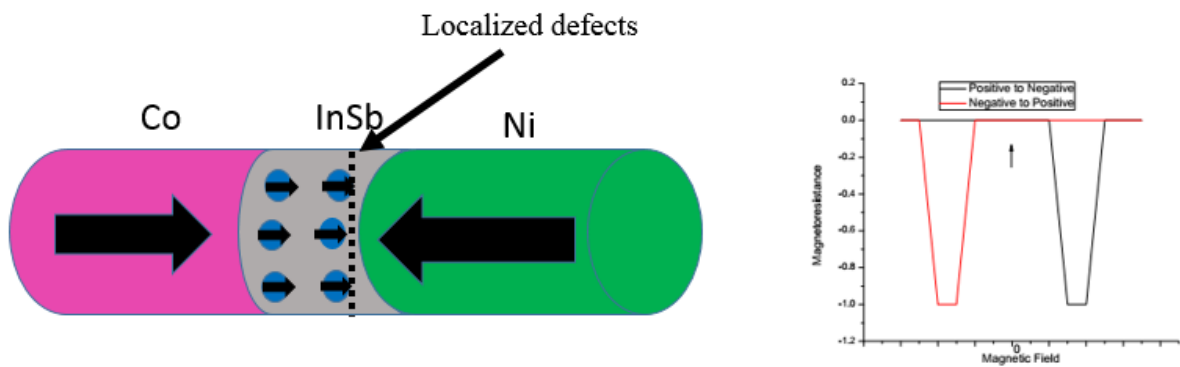


Figure 1-2: Inverse spin valve effect in the presence of localized defects

### 1.1.2 Hanle Oscillation

In the Hanle effect, the conductance of a spin valve structure oscillates with a magnetic field applied transverse to the direction of current flow (figure 1-3).

If a magnetic field is applied in a transverse direction with respect to the magnetic polarization of the ferromagnetic contacts as shown in figure 1-3 (the field is small enough to not change the polarization of the ferromagnetic contacts) then spins of the injected electrons will precess

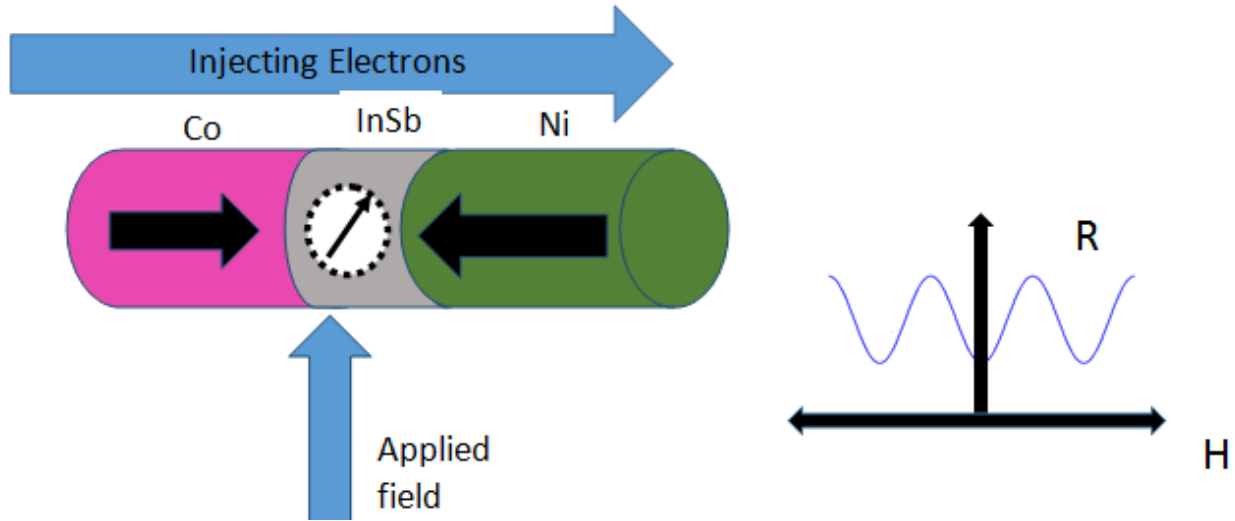


Figure 1-3: Hanle Oscillation. The resistance is oscillating with applied field

about the axis of applied field because of Larmor precession. If the contacts' magnetizations are antiparallel to start with (figure 1-3), the structure will exhibit a higher resistance when the precession is even multiple of  $180^\circ$  ( $2n \cdot 180^\circ$ ,  $n$  is an integer) and a lower resistance when the precession is an odd multiple of  $180^\circ$  ( $(2n+1) \cdot 180^\circ$ ,  $n$  is an integer). The precession rate is dependent on the applied field ( $\frac{d\phi}{dt} \sim B$ ). Hence, if we scan the transverse field, we will change the angle by which the spins precess in traversing the spacer layer. As a result, the conductance will oscillate as we scan the field. The period of the oscillation is given as,  $B_{period} = \frac{h}{|g|\mu_B \langle \tau_t \rangle}$  where  $\langle \tau_t \rangle$  is the average transit time of electrons through the spacer. We will see the same oscillations if the ferromagnetic contacts had been initially aligned in the parallel direction,

although this time an even multiple of  $180^\circ$  rotation will produce the maximum resistance and an odd multiple will produce the minimum.

Clearly neither the Hanle effect, nor the spin valve effect can be observed unless the ferromagnetic contacts act as spin polarizers and analyzers. Nor would they be observed if spin transport within the InSb layer was not somewhat coherent (i.e. the spin polarization is not being completely randomized by spin relaxation events). Therefore, the observation of these two effects is a confirmation of successful injection, detection and coherent transport of spins.

## 1.2 SPIN RELAXATION MECHANISM

In this section, some of the major spin relaxation mechanism in a solid will be discussed.

### 1.2.1 E-Y Mechanism

In a crystal, the Bloch states are not spin eigenstates. This makes the spin orientation of an electron a function of its wavevector. This situation is schematically shown in figure 1-4. [1]

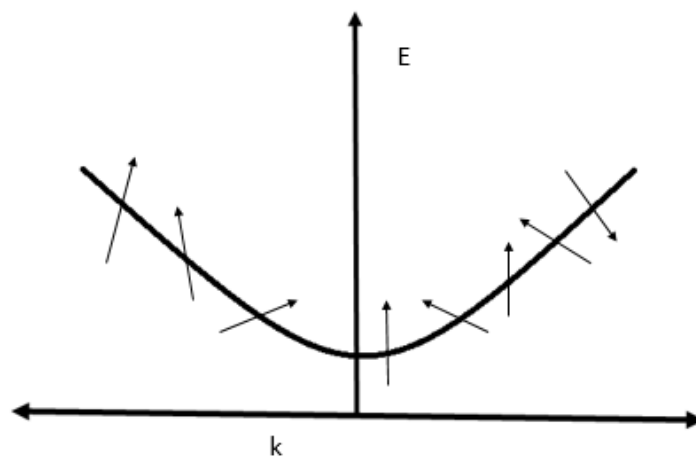


Figure 1-4: Spin polarizations at different wavevectors in an energy-wavevector dispersion relation

As a result, whenever an electron suffers a momentum relaxing scattering event due to phonons, impurities, etc., the spin polarization of the electron changes owing to the change of the momentum (wavevector). This spin relaxation mechanism is called Elliott-Yafet mechanism. Naturally, the spin relaxation rate in this mechanism is directly proportional to momentum relaxation rate.

### 1.2.2 Spin Orbit interaction and D'yarkonov Perel' Spin Relaxation Mechanism

In a single atom, when an electron is orbiting around the nucleus with a velocity  $\vec{v}$ , it will feel the electric field due to positively charged nucleus. In the rest frame of the electron, this electric field is converted to a magnetic field through Lorentz transformation. The resulting magnetic flux density experienced by the electrons is

$$\vec{B}(\vec{v}) = \frac{\vec{E} * \vec{v}}{2c^2 \sqrt{1 - \frac{v^2}{c^2}}} \dots \dots \dots (1.1)$$

where  $c$  is the speed of light in vacuum.

Classically, we can view the spin of the electron as being associated with self-rotation about its own axis. If the magnetic moment of the self-rotating electron is written as  $\vec{\mu}_e$ , then the energy of its interaction with  $\vec{B}$  is-

$$E_{rel} = -\vec{\mu}_e \cdot \vec{B} \dots \dots \dots (1.2)$$

This interaction is called spin-orbit interaction:  $\vec{\mu}_e$  is associated with the spin and  $\vec{B}$  with the orbital motion.

In a solid, conducting electrons are not strongly attracted to the nuclei; rather, they are quasi free. Nevertheless, an electron will see an electric field due to either internal effects (such as space charges) or external applied field. That will also induce a spin orbit interaction field.

If the spin orbit interaction is created by an internal potential gradient (conduction band discontinuity in hetero structure) or due to an electric field, this interaction is called Rashba interaction. If the internal field is created due to crystallographic inversion asymmetry in a crystal, the associated spin orbit interaction is called Dresselhaus interaction[1]. In either case, the spin orbit interaction acts like an effective magnetic field and this field is velocity dependent [see Equation (1.1)].

The effective magnetic field arising from spin-orbit interaction causes a spin to precess about itself. This is called Larmor precession and the precession frequency is

$$\vec{\Omega}(\vec{v}) = \frac{e\vec{B}(\vec{v})}{m^*} \dots\dots\dots(1.3)$$

If all the electrons move with the same velocity, then they will all experience the same effective magnetic field due to spin-orbit interaction and therefore their spins will be rotated by exactly the same angle over a fixed duration of time owing to Larmor precession. Additionally, because they all have the same velocity, they will all have exactly the same spin polarization at any fixed distance from the injection point. Consequently, there will be no spin relaxation due to spin-orbit interaction. But if the velocity  $\vec{v}$  changes randomly with time due to scattering, different electrons would have been precessed by different angles. So even if all the electrons are injected with the same spin polarization, the net spin polarization will be randomized gradually, resulting in loss of spin coherence of the electron ensemble. This is the D'yakonov-Perel' (DP) spin relaxation mechanism[1]. In a strictly one dimensional nanowire where only a single subband is

occupied, the direction of  $\vec{v}$  is fixed; it is along the axis of the wire. Although the magnitude of the velocity can vary owing to inelastic scattering and thermal spread in energy, the direction remains fixed. Hence the direction of the effective magnetic field  $\vec{B}(\vec{v})$  is fixed. The spin precession axis therefore always remains the same for all electrons, regardless of their scattering history, and hence the DP relaxation is absent in a strictly one-dimensional quantum wire[6].

### 1.3 MAGNETO-RESISTANCE

Magnetoresistance is a phenomenon where the resistivity of a sample changes in an applied magnetic field. There are many origins of magnetoresistance, some related to spin and others not. In this thesis, we have studied two specific magnetoresistance effects – one related to spin and the other not. The former is anisotropic magnetoresistance (AMR) that arises from spin-orbit interaction in a ferromagnet that makes the resistivity of the ferromagnet depend on the angle between the direction of current flow and its magnetization. This effect is strain sensitive. We were able to generate strain in the ferromagnetic contacts of a spin valve by heating with an infrared lamp. The strain was caused by unequal thermal expansion of the ferromagnet and the underlying substrate. We found that strain significantly enhances the AMR effect.

An intriguing giant magnetoresistance effect was discovered in a nanowire structure that is not a spin valve. It consists of a copper nanowire with gold contacts. A transverse magnetic field (perpendicular to the direction of current flow along the wire) pushes electrons in the Cu nanowire toward one edge because of the Lorentz force, so that electron accumulation takes place at one edge and depletion at the other. This is the same phenomenon that causes the classical Hall effect. Because of atmospheric oxidation of Cu, there is always a thin CuO layer interposed between the Cu and Au that acts as a potential barrier for electrons at the wire/contact



interface since CuO is a semiconductor with a bandgap between 1.66 eV and 2.54 eV. This barrier's height is reduced at the accumulated edge and raised at the depleted edge because of the relative shift in the Fermi level with respect to the conduction band edge of Cu (caused by increase in the electron concentration at the accumulated edge and decrease at the depleted edge). The modulation of the barrier heights by a magnetic field changes the conductance dramatically (a lower barrier increases the thermionic emission and tunneling rates while a higher barrier decreases them) and gives rise to a giant magnetoresistance.

#### **1.4 ORGANIZATION OF THE THESIS**

The remainder of this thesis is a collection of the experimental details and results pertaining to spin transport and magnetic behavior of electrons in 1D quantum wires. Several growth techniques (such as Electrochemical Self Assembly, resistive evaporation), fabrication techniques, nano characterization techniques (SEM, TEM, AFM, VSM etc.), measurement techniques (I-V, B-R etc.) have been used in undertaking the experiments , which will be discussed.

Chapter 2 describes the demonstration of injection, coherent transport and detection of spins in tri-layered nanowires called “spin valve”, where an InSb layer is sandwiched between two ferromagnetic contacts, Co and Ni. The spin relaxation time/length in InSb has been extracted from experiments which showed a significant (10-fold) increase in the nanowire compared to bulk or quantum well.

In chapter 3, the mechanism of modulating spin relaxation with infrared light is discussed, which offers the possibility of a spintronic IR detector. It can ideally have infinite light to dark contrast

ratio and zero dark current resulting in zero standby power dissipation. The proposed idea is exemplified with a simple experiment where the resistance of a spin valve structure has been modulated with light without causing electron-hole pair generation. The modulation is entirely due to spintronic effects.

In chapter 4, I report the observation of a giant magneto-conductance in a single nanowire. The origin of this effect lies in the modulation of a potential barrier that forms at the nanowire/contact interface with a magnetic field. The magnetoresistance is 10,000,000%, which far exceeds that observed in typical GMR based read heads (few hundred percent).

In chapter 5, spin transport across a single metal nanowire (captured between two ferromagnetic contacts) was inspected. We observed no AMR effect in the dark and a strong AMR under intense infrared illumination. The effect increases when the light source is brought closer to the sample. This is not an optical effect, but a heating effect. The light source heats the ferromagnetic contacts and strains them because of the unequal thermal expansion of the contacts and substrate. The strain enhances the AMR effect.

## **2 COHERENT SPIN TRANSPORT IN NANOWIRE SPIN VALVES:**

---

In this chapter, I will discuss about the experiments to probe coherent spin transport in a 1D InSb channel. InSb is the material of choice for two reasons: (1) InSb has high Rashba spin orbit interaction (SOI) because of its low bandgap. A high Rashba SOI is necessary to implement spintronic devices like the Datta-Das Transistor. [1] , but it also causes increased spin relaxation. That is why it is important to seek ways to suppress spin relaxation in a material like InSb. Fortunately, if all the electrons in a 1D wire can be confined to the lowest subband, then the major spin relaxation (D'yakonov-Perel') can be eliminated [6] in any semiconductor. Because InSb has a small effective mass, in a 50nm diameter InSb channel, about 96% of the electrons occupy the lowest subband at room temperature. This results in successful suppression of the D'yakonov-Perel' (DP) relaxation and a concomitant increase in the spin relaxation time.

In the following sections, I have described fabrication of InSb nanowires, followed by experimental measurement of spin transport. Finally, I have analyzed the data and drawn conclusions.

### **2.1 EXPERIMENTAL SETUP:**

In this section, the sample growth mechanism and measurement setup will be discussed.

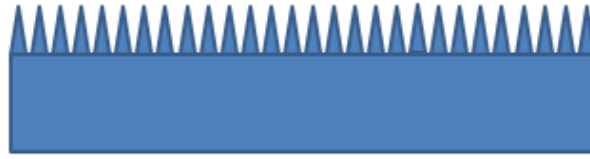
#### **2.1.1 Sample Growth and Characterization:**

We start with an ultrapure (99.99%) 100 $\mu$ m thick aluminum foil sourced from Alfa Aesar (figure 2-1.a). The foil is electropolished in a solution containing Perchloric acid, Butyl

Cellusolve, Ethanol and distilled water to reduce the root-mean square surface roughness from 50nm to 3nm [7], [8].

In electropolishing, the work piece is immersed in the above mentioned electrolyte and acts as anode. A current is passed through this anode, which causes the metal surface to be oxidized and dissolved in the electrolyte. The protruding part oxidizes and dissolves faster, causing the whole surface to be flat (figure 2-1.b). On the other hand, in the cathode, Hydrogen gas is formed due to the reduction. This method of levelling is called anodic levelling.

The polished surface is then anodized in 3% Oxalic acid at 40V for 45 minutes. This creates a porous alumina ( $\text{Al}_2\text{O}_3$ ) layer on top of the Al foil which is used as the template to create nanorods (figure 2-1.c). The length of anodization time varies, depending upon the required length of nanorods. In the as-anodized film, the diameter of the pores is around 30 -40 nm. At the bottom of the pore, there is a thin  $\text{Al}_2\text{O}_3$  layer that acts as an insulating barrier to DC electrodeposition of materials selectively within the pores. To make this barrier layer thinner, the anodization process is terminated gradually. The anodization voltage is gradually reduced from 40V to 15V and kept at that voltage for 15 minutes. This process thins down the barrier layer [7]. Figure 2-2 shows how anodization current behaves in different stages of the process. Next, to remove the thinned barrier layer completely, the anodized foil is soaked in 5% phosphoric acid for about an hour. Since the acid etches isotropically, it not only removes the barrier layer, but also widens the pores. The etching time has to be carefully adjusted, as widening pore diameters also results in decreasing the inter-pore distance. At the end of this process, the pores widen up to 50-60 nm diameter.



(a)



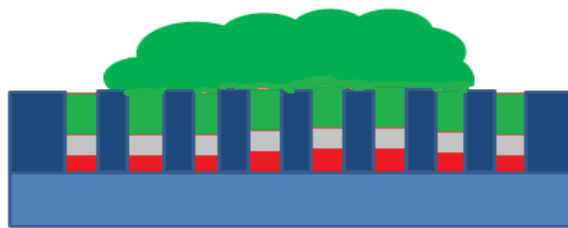
(b)



(c)



(d)



(e)

Figure 2-1 : (a) 100 μm thick rough Al foil. (b) Flat surface after electropolishing. (c) Porous Al<sub>2</sub>O<sub>3</sub> on top of Al foil. (d) Bottom barrier layer is removed using 5% Phosphoric acid. (e) The pores are filled selectively with Co, InSb and Ni respectively

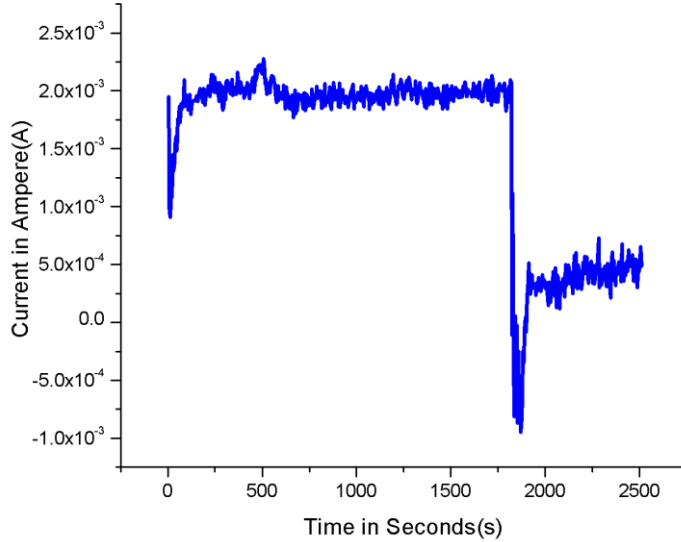


Figure 2-2: Anodization current vs. Time behavior during anodization

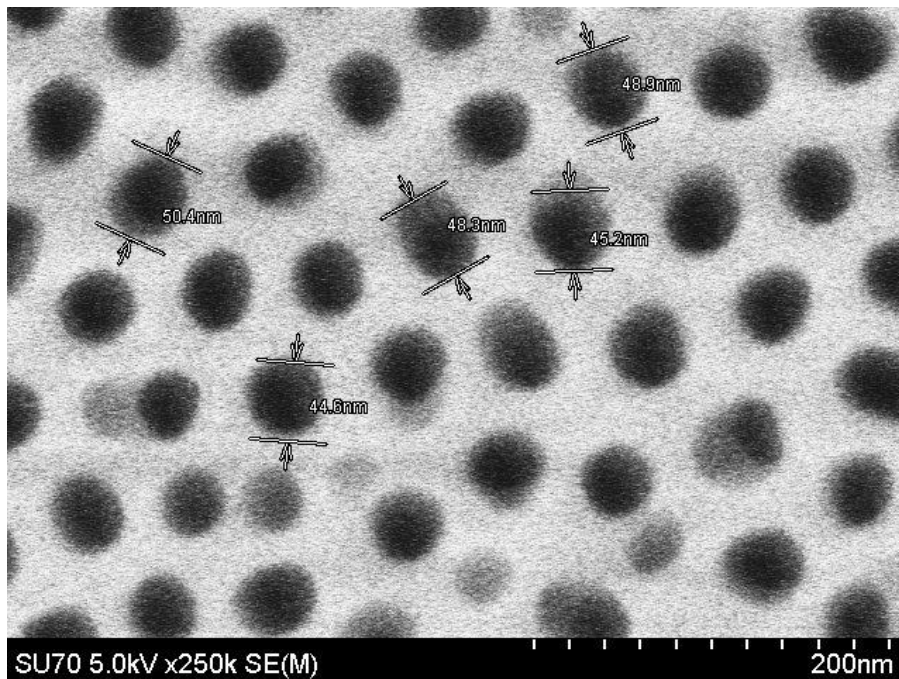
In figure 2-3, the SEM images show the alumina templates at different stages. Figure 2-3.a and 2-3.b show the alumina templates from the top view and cross sectional view respectively. Figure 2-3.c, which is an inverted image shows the barrier layer, which is schematically shown in figure 2-1.c. Figure 2-3.d shows the bottom of the template once the barrier layer is removed (corresponding to figure 2-1.d)

After removing the barrier layer, the pores are filled with required material with DC electrodeposition. The spin valve requires a tri-layer nanowires, which is done by depositing Co, InSb and Ni respectively. The electrolyte for Co deposition consists of 28.09 gm of  $\text{CoSO}_4 \cdot 7\text{H}_2\text{O}$  and 7 gm of Boric acid in 1 liter of distilled water. The electrolyte of InSb consists of 0.15M  $\text{InSO}_4$ , 0.1M  $\text{SbCl}_3$ , 0.17M  $\text{Na}_3\text{C}_6\text{H}_5\text{O}_7$  and 0.36M  $\text{C}_6\text{H}_8\text{O}_7$  (Citric acid) dissolved in distilled water.[9] Ni's electrolyte consists of 26.27 gm of  $\text{NiSO}_4 \cdot 6\text{H}_2\text{O}$  and 7 gm of Boric acid dissolved in 1 liter of distilled water. Boric acid is used to increase the conductivity of the solution. The Co and InSb deposition was carried out for 1 minutes each and Ni deposition was done at 5V for 6

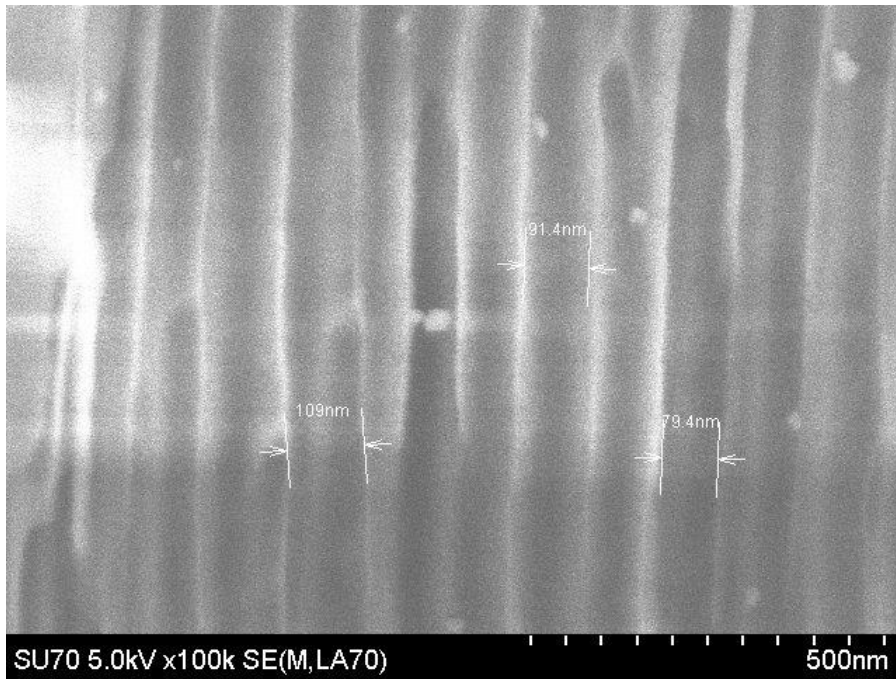
minutes to make sure that the pores are filled up to the brim. Figure 2-1.e shows the schematic of over deposited Alumina template.

To make contacts for electrical measurements, gold wires were used. The gold wires were attached on top of the sample surface and the bottom of the Al foil using silver paste. The nanowire density is  $10^{10} \text{ cm}^{-2}$  and the contact area is about  $1\text{mm} \times 1\text{mm}$ . So about  $10^8$  nanowires are covered by the top contacts and hence electrically probed. In the overfilled areas, all the wires should be electrically connected. But in the under filled areas, only a fraction of the wires are actually connected.

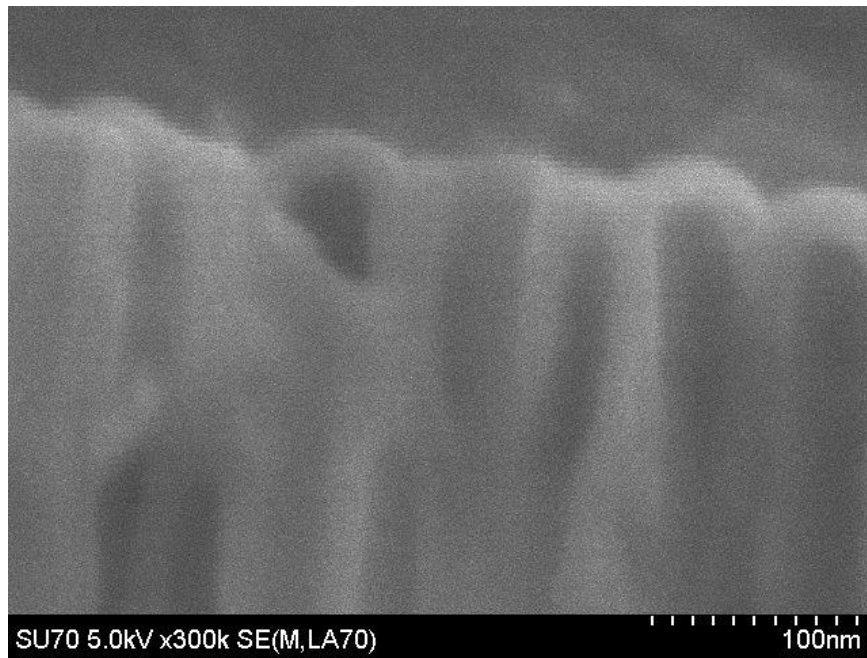
The elemental composition of the nanowire spin valves was verified using energy dispersive x-ray spectroscopy (EDS). Distinct peaks for Co, Ni, In and Sb were found as expected since they are constituents of the spin valves (Figure 2-4).



(a)

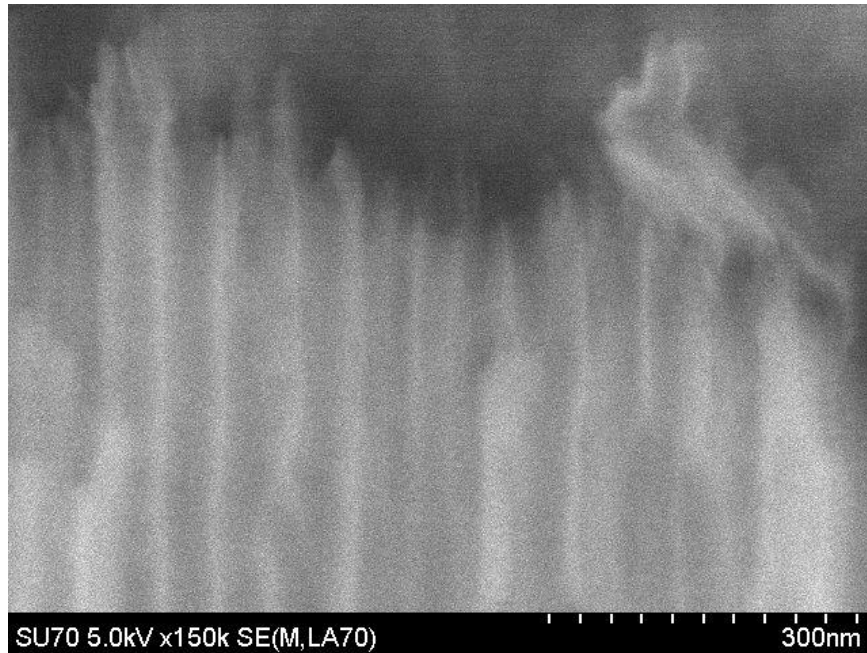


(b)



(c)





(d)

Figure 2-3: (a) Top View of the Alumina ( $\text{Al}_2\text{O}_3$ ) template (b) Cross Sectional View of the Alumina ( $\text{Al}_2\text{O}_3$ ) template (c) Barrier layer at the bottom of the Alumina ( $\text{Al}_2\text{O}_3$ ) (d) Removal of the Barrier layer with 5% Phosphoric Acid

We have also found peaks for Al and O originating from the Alumina templates in the EDS spectra.

The magnetization curves (Magnetic moment vs Magnetic Field) for porous Alumina filled with Co (deposited for 30 seconds) and Ni (deposited for 4 minutes) separately have been obtained using Vibrating Sample Magnetometer (from Quantum Design). The magnetic field was applied along the nanowire/pore axes. These curves confirm that the nanocontacts are indeed ferromagnetic and have non-zero remanence, although they have a small coercivity. The measurement was done at room temperature (Figure 2-5.a, 2-5.b).

The TEM imaging has been done to show the 3 layers of the spin valve and also to determine the InSb spacer layer. Co and Ni have atomic densities close to  $9.1 \times 10^{22} \text{ cm}^{-3}$  and InSb has an atomic density close to  $2.94 \times 10^{22} \text{ cm}^{-3}$ . Since we have carried out bright field imaging, InSb region was more transparent than the Co and Ni layer. In both SEM and TEM, the diameter of the wire has been found around 50 nm. The TEM sample was prepared by dissolving the alumina matrix in 1.25M NaOH and then the TEM grid was soaked in the liquid to capture the released nanowires. The grid was subsequently soaked into distilled water to dilute the NaOH and then dried in vacuum chamber (Figure 2-5.c).

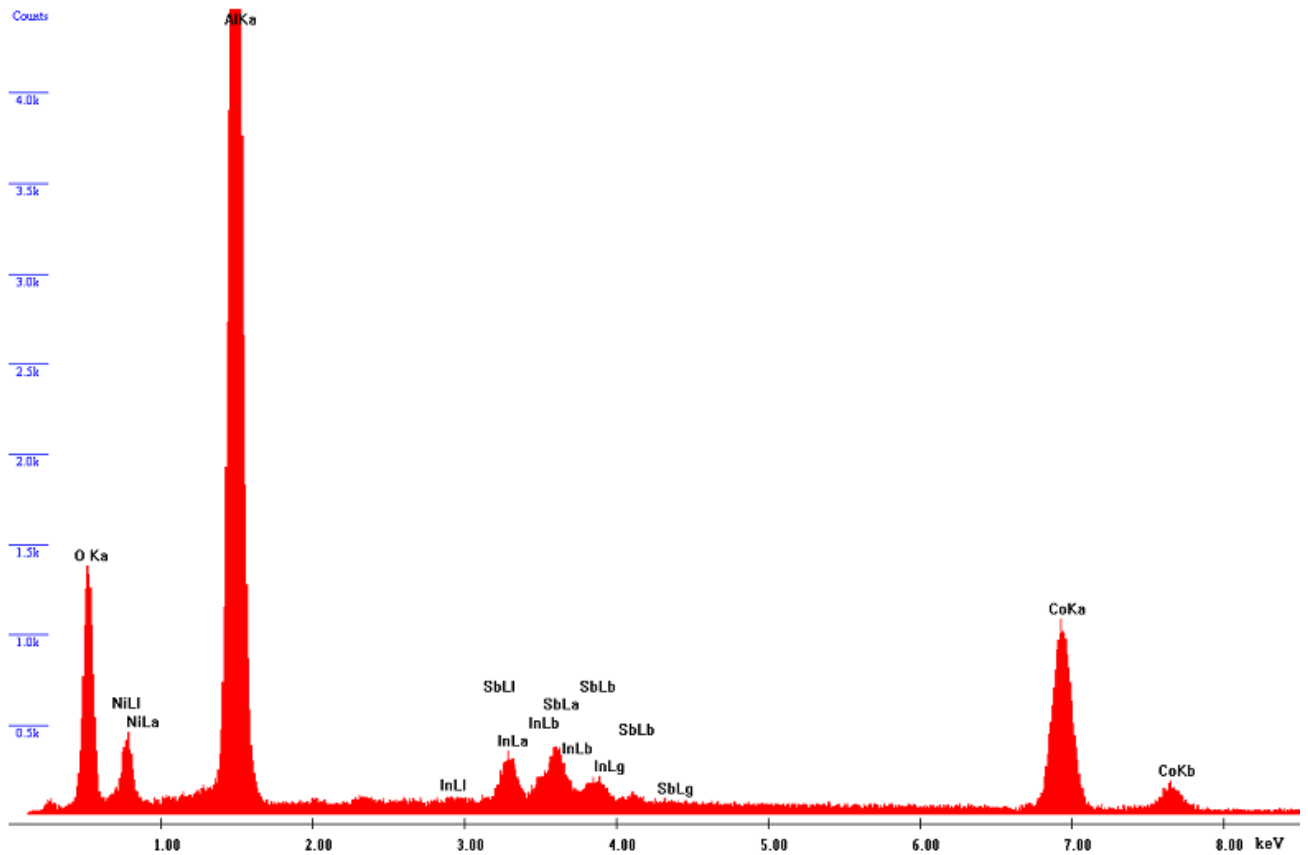
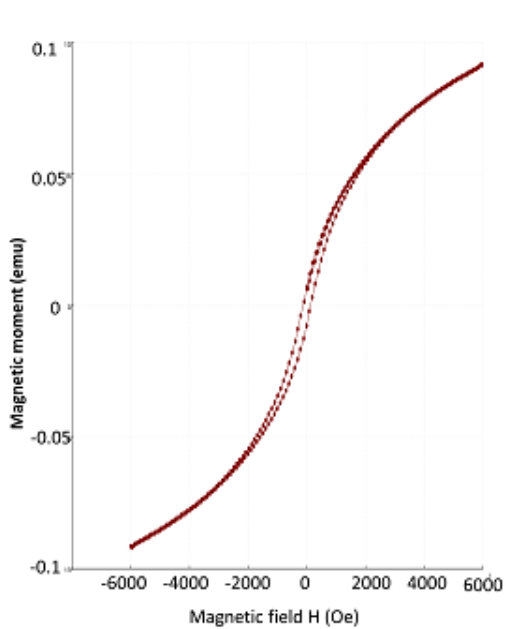
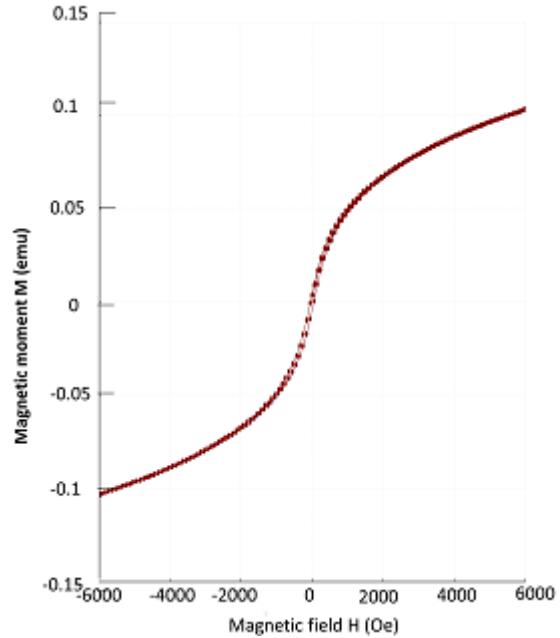


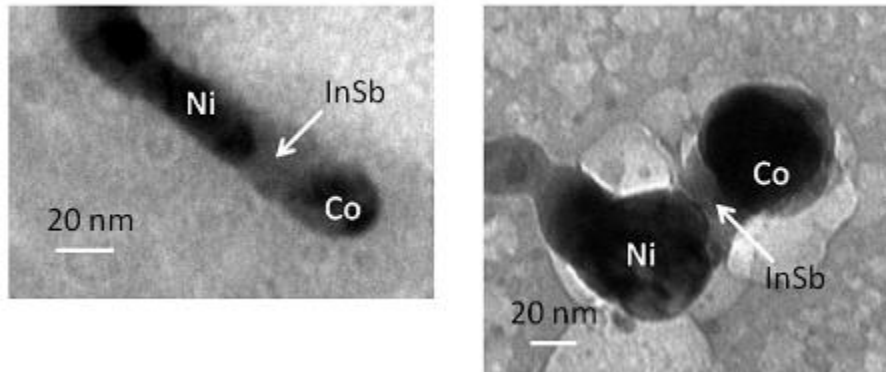
Figure 2-4: EDS of spin valve samples



(a)



(b)



(c)

Figure 2-5:(a),(b) Magnetization curve for Co and Ni using VSM (c) TEM images of a single tri-layer nanowire using bright field imaging

## 2.1.2 Measurement Setup:

For longitudinal magnetoresistance measurement, the samples were mounted between the pole pieces of an electromagnet. The magnetic field was directed parallel to the nanowire axes and set

to 4000 Oe to magnetize both cobalt and nickel layers along their major axes. The field was then abruptly reduced to 0 Oe and scanned towards the opposite direction in steps of -43 Oe. In every step, the resistance was monitored with a resistance meter at room temperature. After reaching -4000 Oe, the field again abruptly reduced to zero and scanned in the positive direction with the same step size and up to 4000 Oe.

For transverse magnetoresistance measurement to observe the Hanle effect, the samples were rotated 90 degrees in the magnetic field. The magnetic field is then scanned from -1000 Oe to +1000 Oe, both limits being well under the coercive fields of the contacts. This ensures that the transverse field does not flip the magnetizations of the contacts which are aligned along the wire axis. From the longitudinal magnetoresistance measurement, the coercivities for both Co and Ni contact were found to be more than 1500 Oe. The transverse magnetoresistance was measured in the same fashion as the longitudinal magnetoresistance.

The experimental setup is shown in figure 2-6.

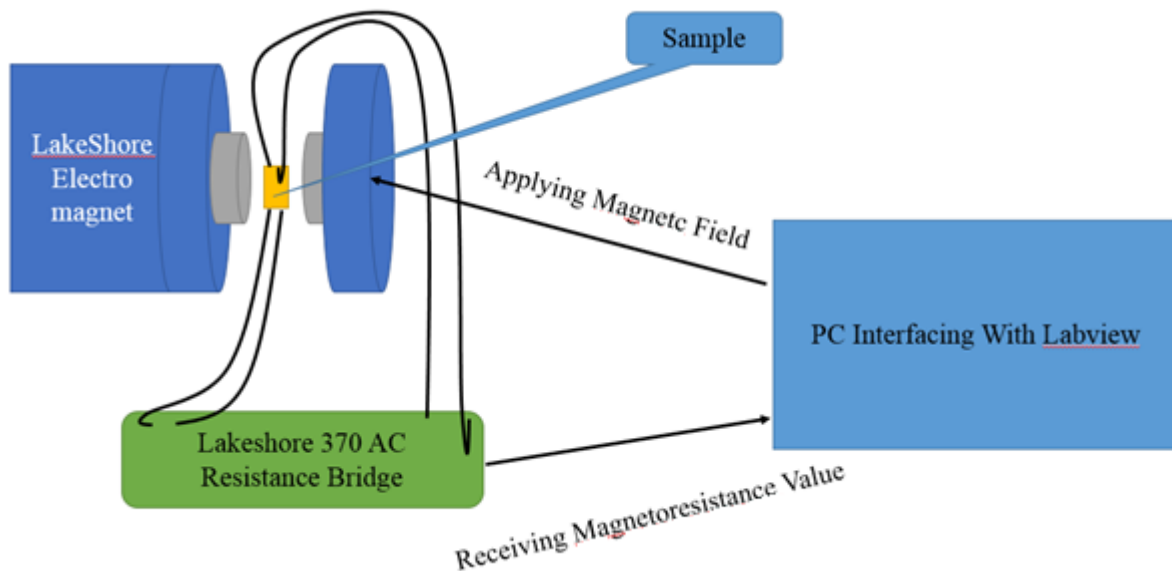


Figure 2-6: Experimental setup for magnetoresistance measurement

## **2.2 OBSERVING THE SPIN VALVE EFFECT AND THE HANLE OSCILLATION:**

Longitudinal magnetoresistance (magnetic field directed parallel to wire axis) plots with respect to applied field are obtained in 3 different samples at room temperature and are shown in figure 2-7. Distinct troughs can be observed in all 3 samples. In sample 1 and 2, the position of the troughs are consistent with the literature, [10] [11] but sample 2 shows troughs at very low fields. This is possibly because, in sample 2, the pores were overfilled with Ni, hence a thick layer of Ni was formed, which acted like a bulk Ni. Bulk Ni has coercivity of around 20 Oe.[12] In our sample 2, we also see that the coercivity has been dropped to 50 Oe, which supports our overfilling hypothesis. SEM images provide further proofs to support this assumption. (Figure 2-8) The presence of troughs however confirms the presence of the spin valve effect.

The interesting point to be noted here is that since Ni and Co both have negative spin polarizations, we were supposed to observe magnetoresistance peaks rather than troughs. The reason that we are seeing troughs is because of the inverse spin valve effect that has been seen before and explained. [5], [13] If electrons tunnel through resonantly via one or more localized defect sites in InSb spacer layer whose energies match the Fermi energy of the ferromagnetic electrodes, then it will effectively invert the spin polarization of the ferromagnetic closer to the defect site. Such behavior has been observed in ferromagnetic/paramagnetic nano junctions of cross sections smaller than  $0.01 \mu\text{m}^2$  grown by electrodeposition, as is the case here. [5]

We also observe an increasing background magnetoresistance. This is expected in narrow gap semiconductors like InSb owing to the strong non-parabolicity of the conduction band. The

increasing magnetic field increasingly flattens out the energy-wavevector dispersion relation in a nanowire, causing the effective mass to get higher with increasing field, and hence the positive background magnetoresistance.[14] There was also a thermal drift in the resistance, contributing further to the positive background magnetoresistance.

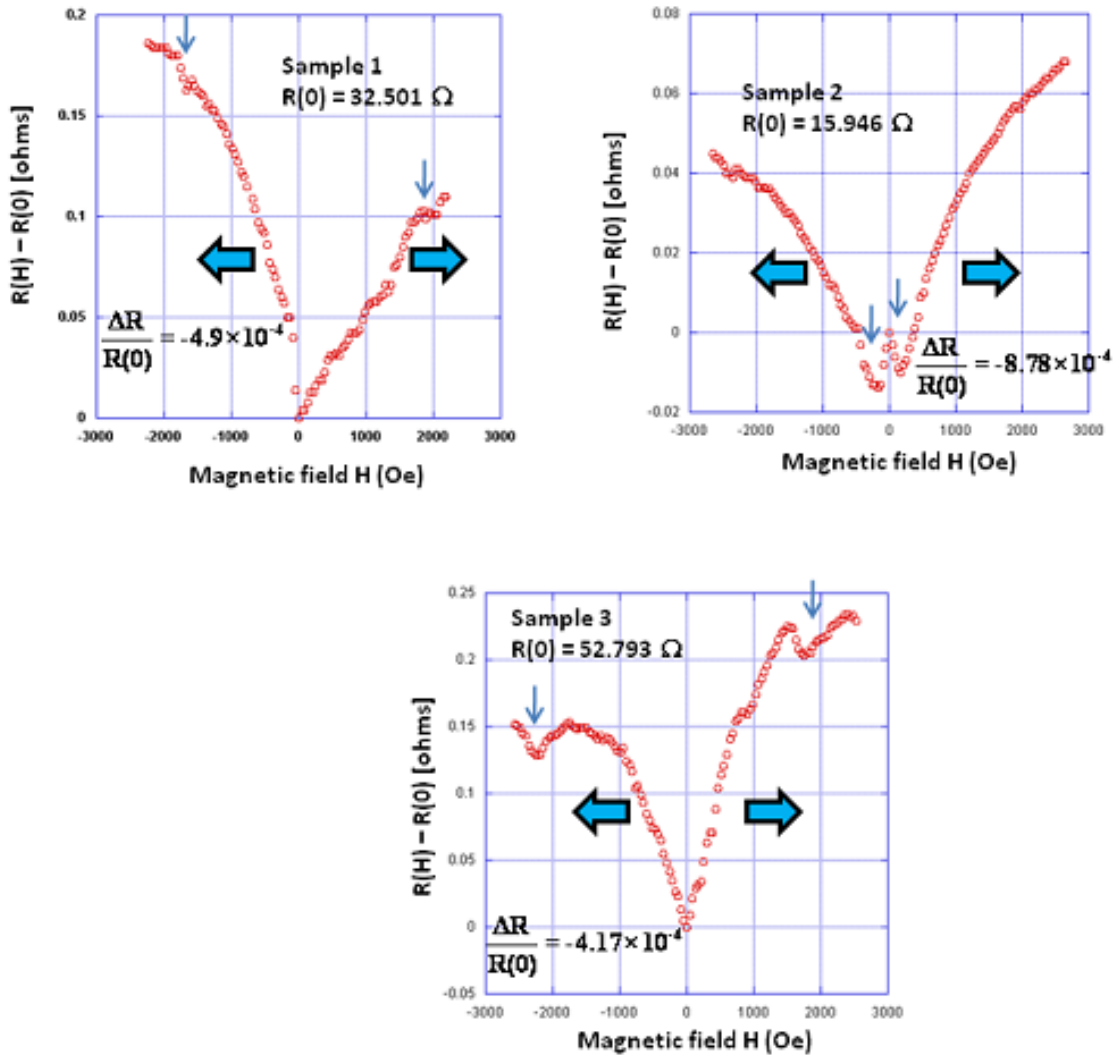


Figure 2-7: The inverse spin valve effect. Room temperature (295 K) longitudinal magnetoresistance plots of three samples showing spin valve troughs. The magnetic field is applied along the axes of the nanowires. The trough positions are indicated with vertical arrows. The horizontal block arrows show the directions in which the field is scanned. The troughs are not symmetric about the resistance axis because of the inevitable asymmetric shapes of the magnets, which make the coercivities of both cobalt and nickel contacts depend on the field direction.

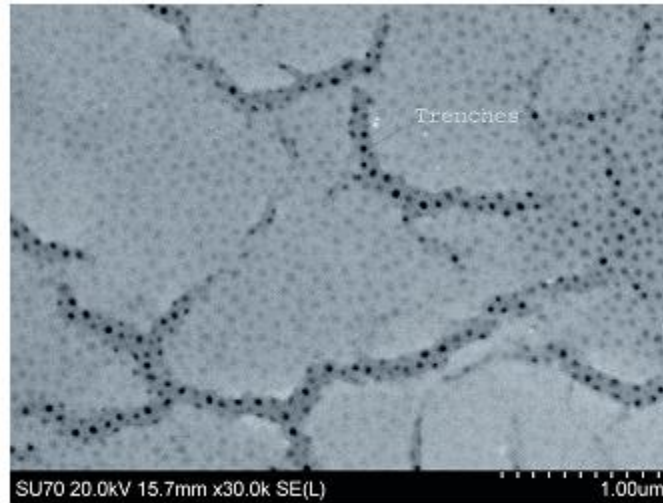


Figure 2-8: Scanning electron micrograph of the top surface of a sample where most nanopores have been overfilled, resulting in the nickel spilling out on the surface to form a thin film. The nickel film segregates, forming narrow trenches where the pores are not filled to the brim. Since the nickel contact is essentially a thin film in these samples, its coercivity plummets to  $\sim 50$  Oe since nickel thin films have very low room temperature coercivities of about 20 Oe.

The transverse magnetoresistance of the samples is then measured in a magnetic field perpendicular to the axis of the wires. The magnetic field value was chosen carefully (from the spin valve experiment) so that it does not exceed the coercivities of Co and Ni. Here, the nanocontacts inject electrons which have spins parallel to the wire axis. These spins will precess about the perpendicular field while traversing the InSb layer. Since Ni and Co contacts are effectively aligned antiparallel to each other, if the spins precess through an angle that is an odd multiple of  $\pi$ , electrons will transmit. On the other hand, if the angle is even multiple of  $\pi$ , electrons will be blocked. Thus the resistance of the sample will oscillate periodically with the applied magnetic field, since the angle of precession is proportional to the transverse field. This is the Hanle effect.[15]–[18] The period of the oscillation (in magnetic flux density) is expressed

as  $B_{period} = \frac{h}{|g|\mu_B\langle\tau_t\rangle}$  where  $\mu_B$  is the Bohr magneton and  $g$  is the Lande g-factor of the InSb spacer material.

Figure 2-9 shows the transverse magnetoresistance plots of samples 1 and 3. Sample 1 shows a distinct periodic oscillation in the resistance/conductance (equally spaced minima and maxima) with a period of  $\sim 315$  Oe which is a clear indication of the Hanle effect. Sample 3 shows a muted oscillation, but still maxima/minima can be discerned with a period of  $\sim 500$  Oe. Sample 2 does not show any oscillation since it has very low coercivity for the observation of Hanle effect. The oscillations are considerably distorted from sinusoidal, because different nanowires have different periods and  $10^8$  nanowires are being probed simultaneously. Ensemble averaging over  $10^8$  periods distorts the shape of the oscillation, making it look non-sinusoidal.

The difference in period between different nanowires accrues from the different transit times  $\tau_t$  that electrons experience in different nanowires. Variations in transit time,  $\tau_t$  are due to two reasons. First, the spacer layers of different nanowires are not exactly equal in length. From the TEM observations, we have found that  $L$  varies by 25%-35%. Second, different electrons in the same spacer layer can travel with different velocities because of thermal broadening and random scattering. Fortunately, this velocity spreading is minimum due to resonant tunneling. Because of it, electrons who have energies very close to resonant level (due to localized impurities), will tunnel through. Thus resonant tunneling is acting as a velocity filter.

If the variation in spacer layer width and velocities are somewhat peaked, we will be able to observe the periodic behavior (as in this case), but the oscillation will be non-sinusoidal.

Another important feature of figure 2-9 is that Hanle oscillation is not symmetric about the zero transverse field, since there is clearly some offset. Our experimental set up made it impossible



for us to align the field perfectly perpendicular to the wire axis. Moreover the wires themselves are not completely parallel to each other, since our Al foil can easily bend. Finally, the magnetizations of the two contacts also may not be completely linear. All these effects can cause an offset.

The period of Hanle Oscillation should however still scale approximately as  $1/\sin\theta$ , where  $\theta$  is the angle between the wire axis and the magnetic field. This indeed happens, the result is shown in figure 2-10.

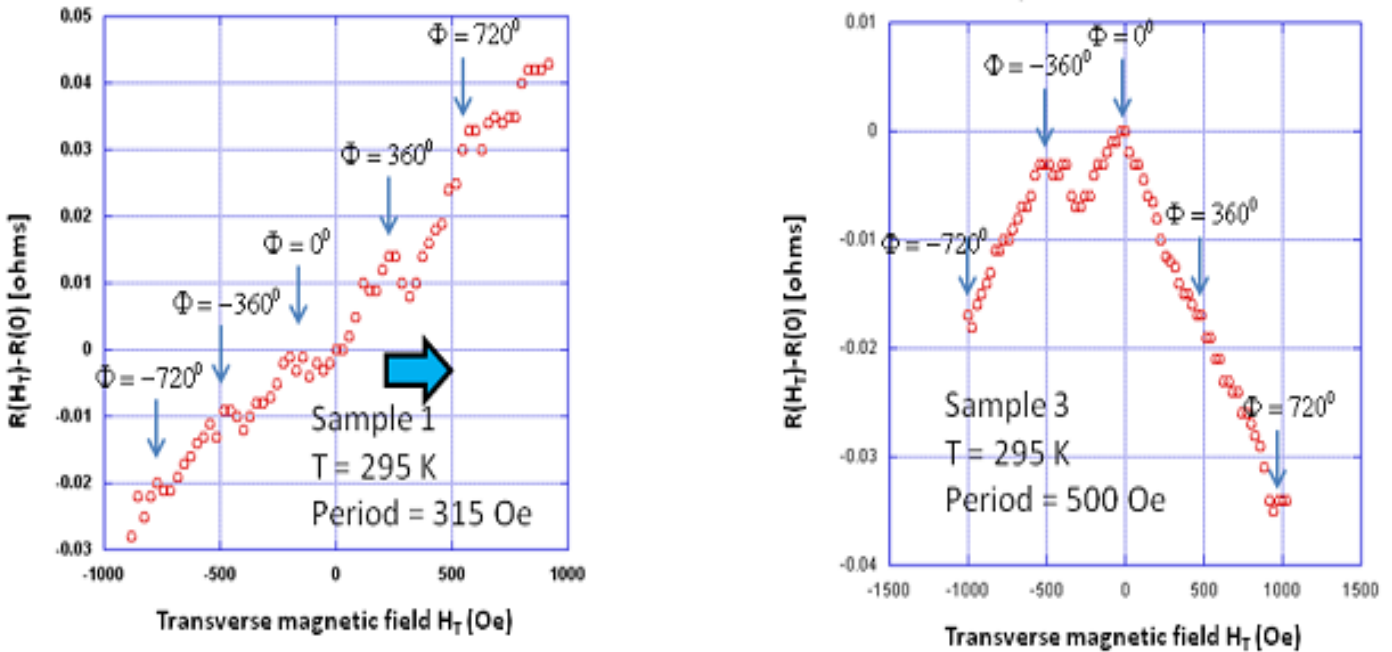


Figure 2-9: Hanle oscillations. Room temperature (295 K) transverse magnetoresistance plots of two samples showing oscillations due to the Hanle effect. The resistance maxima are indicated by arrows and the angle of spin precession is the quantity  $\Phi$ . In sample 1, there is a zero-offset in  $\Phi$  and the maximum closest to zero field is chosen for  $\Phi = 0$ . The block arrow shows the direction of field scan.

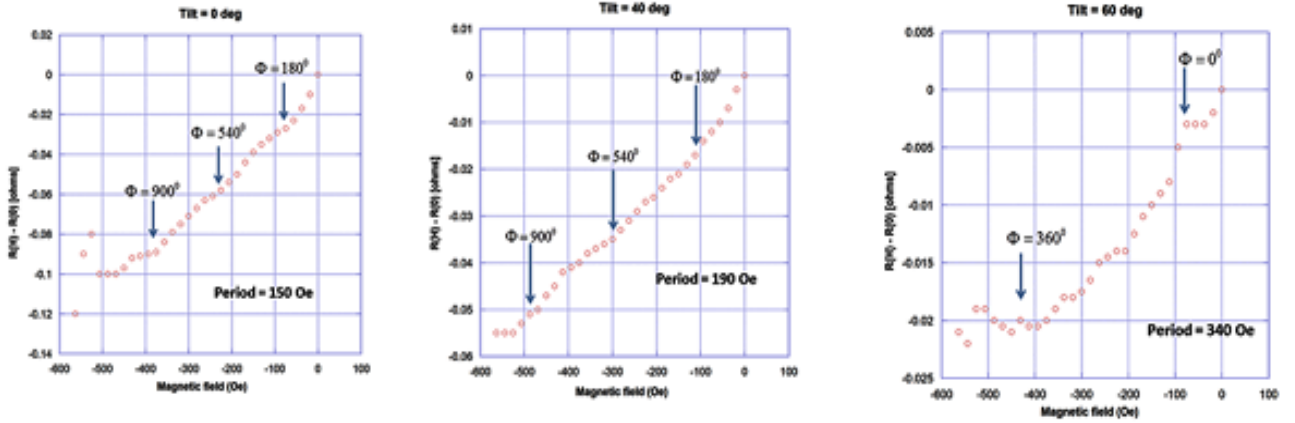


Figure 2-10: Hanle Oscillation for three different tilt angle

In sample 1 and also in the sample of figure 2-10 (intended to check the  $1/\sin\theta$  variation) we saw the resistance increase. This is due to thermal drift. In case of sample 3, we saw the resistance decrease as the magnetic field goes higher. The reason could be that with increasing magnetic field, energy separation between any two subbands increases. Hence the higher band increasingly depopulates as the magnetic field is scanned and electrons transfer from higher to lower band. Although, in our 1D system, 96% of electrons are already residing in the lowest subband and hence the effect of these extra electrons should be negligible, yet as the resistance change is only 0.05%, we cannot neglect this contribution.

### 2.3 SPIN RELAXATION LENGTH IN 1D INSB NANOWIRE

One can relate the magnitude of the trough  $\Delta R$  in the longitudinal magnetoresistance to the spin relaxation length in the InSb spacer layer by invoking the modified Julliere formula [19] which is-

$$\frac{\Delta R}{R(0)} = \frac{2P_1P_2e^{-\frac{L}{L_s}}}{1-P_1P_2e^{-\frac{L}{L_s}}} \dots\dots\dots(2.1)$$

Where  $R(0)$  is the resistance of the structure at zero magnetic field,  $P_1$  and  $P_2$  are the spin polarizations of the two magnetic contacts,  $L$  is the separation between the contacts and  $L_s$  is the spin relaxation length.

In 1D InSb nanowire, 96% of the electrons reside in the lowest subband and hence we have almost a true one dimensional system. [20] Therefore we can write,  $L=v_d\langle\tau_t\rangle$  and  $L_s = v_d\langle\tau_s\rangle$ , where  $v_d$  is the drift velocity of the electrons,  $\langle\tau_t\rangle$  is the ensemble averaged transit time and  $\langle\tau_s\rangle$  is the ensemble averaged spin relaxation time. Equation (2.1) then reduces to-

$$\frac{\Delta R}{R(0)} = \frac{2P_1P_2e^{-\frac{\langle\tau_t\rangle}{\langle\tau_s\rangle}}}{1-P_1P_2e^{-\frac{\langle\tau_t\rangle}{\langle\tau_s\rangle}}} \dots\dots\dots(2.2)$$

For our Co contacts, we have assumed  $P_1=0.1$  and for Ni,  $P_2=0.075$  .[20] Based on these spin polarization values and measurement of  $\frac{\Delta R}{R(0)}$  from figure 2-7, we have found out that  $\frac{\langle\tau_t\rangle}{\langle\tau_s\rangle} = 3.4$  in sample 1 and  $\frac{\langle\tau_t\rangle}{\langle\tau_s\rangle} = 2.8$  in sample 2 and  $\frac{\langle\tau_t\rangle}{\langle\tau_s\rangle} = 3.6$  in sample 3.

The ensemble average of transit time through the InSb spacer layer is given as-

$$\langle\tau_t\rangle = \frac{h}{|g|\mu_B B_{Period}} \dots\dots\dots(2.3)$$

Here,  $B_{Period}$  can be calculated from our observed data. In InSb quantum dots, the g-factor has been reported to be -52[21] in the lowest subband, which is close to the bulk value -51. Using this equation, we find  $\langle\tau_t\rangle$  equals to 44ps and 28 ps respectively for sample 1 and 3. Again we

previously found  $\frac{\langle\tau_t\rangle}{\langle\tau_s\rangle}$  as 3.4 in sample 1 and 3.6 in sample 3. Hence, ensemble averaged spin relaxation time is 13ps and 8 ps respectively.

The room temperature spin relaxation time in epilayers of InSb has been reported as 2.5 ps [22] and as high as 300 ps[9]. In quantum wells, it drops to 1.2-4.8 ps.[24] It has been suggested theoretically that intrinsic inversion symmetry breaking at the interfaces of a quantum well can decrease spin relaxation time by over an order of magnitude.[25] The calculated spin relaxation time in InAs/GaSb quantum wells is only 0.9 ps. We are using InSb spacer layers with 50nm diameter, so the spin relaxation time should decrease even more due to higher surface to volume ratio. So, the value of  $\langle\tau_s\rangle$  was expected to be around or below 1 ps. But what we have found (13 and 8 ps) is approximately larger by an order.

The mobility within the InSb layer has been found  $2.5-2.8*10^{-4}\text{m}^2/\text{V}\cdot\text{sec}^2$ , which is 4 orders of magnitude smaller than the bulk value( $8\text{ m}^2/\text{V}\cdot\text{sec}^2$ )[26] or even the value in quantum wells. The detailed calculation is shown in the supplementary of [20]. This serious degradation is due to the increased scattering because of the high surface to volume ratio. This degradation of mobility should increase the Elliot Yafet spin relaxation by four orders of magnitude as EY spin relaxation mechanism is inversely proportional to mobility. [27] But what we have found is that spin relaxation rate is decreased by an order. This indicates that: (1) EY is not the dominant spin relaxation mechanism in our system but D'yakonov Perel(DP) is and (2) DP mechanism has been eliminated or suppressed due to the one dimensional confined carrier motion resulting from single subband confinement of electrons.

## 2.4 CALCULATION OF RELATIVE SUBBAND POPULATIONS IN THE NANOWIRES: PROOF THAT 50-NM DIAMETER NANOWIRES HAVE A SINGLE OCCUPIED SUBBAND

The reason for the suppression of DP spin relaxation rate resulting in increased spin relaxation length has been attributed to the single subband occupancy of electrons in an InSb nanowire. In this section, we will theoretically estimate the relative subband occupancies in 50nm diameter of InSb nanowire.

The nanowires are cylindrical in shape, and if we assume that their axes are along the z-direction, then the wavefunctions and energies of electrons in different subbands of the InSb segment are given by [28]-

$$\psi_{n,m}(k_z) = \frac{1}{N} J_N(k_{n,m}r) \exp(in\theta) \exp(ik_z z)$$

$$E_{n,m} = \frac{\hbar^2}{2m^*} (k_{n,m}^2 + k_z^2) \dots \dots \dots (2.4)$$

where  $J_n$  is the Bessel function of n-th order, N is a normalization constant,  $k_z$  is the electron's wavevector component along the wire axis (z-axis),  $m^*$  is the electron's effective mass, and  $r, \theta$  are the radial and angular coordinates on the cylinder's circular cross-section.

In order to find  $k_{n,m}$  we apply the boundary condition that the wavefunction vanishes at the interface between InSb and the surrounding material, i.e. when  $r = R$ , where  $R (= 25 \text{ nm})$  is the nanowire's radius. Therefore, we first find the zeroes of the Bessel function for  $n = 0$ , which yields  $k_{0,1} = 2.4048/(25 \text{ nm}) = 9.6 \times 10^7 \text{ m}^{-1}$ ,  $k_{0,2} = 5.5201/(25 \text{ nm}) = 2.2 \times 10^8 \text{ m}^{-1}$ ,  $k_{0,3} = 8.6537/(25 \text{ nm}) = 3.5 \times 10^8 \text{ m}^{-1}$  and  $k_{0,4} = 11.7915/(25 \text{ nm}) = 4.7 \times 10^8 \text{ m}^{-1}$ . From these values, we compute that the energies of the lowest four subbands are 0.9 kT , 4.8 kT , 12.1 kT and 21.8 kT at room

temperature, since the effective mass of an electron in InSb is 0.0145 times the free electron mass [26]. Therefore, at room temperature, ~96% of the electrons are in the lowest subband of the nanowire, if we approximate the one-dimensional density of states function with a delta function and assume Fermi-Dirac statistics. Thus, we essentially have single subband occupancy and a true InSb quantum wire.

## 2.5 TRANSPORT MODEL IN NANOWIRE SPIN VALVE

A detailed discussion of transport model of electrons in a nanowire spin valve will be helpful to understand how the improved spin relaxation length is benefitting the whole system.

As can be seen in figure 2-11, carrier motion in the nanowire spin valves are dominated by three effects. (1)The Schottky barriers between the two metal-semiconductor interfaces. (2) Drift motion in the semiconductor channel. (3) Resonant tunneling through the point defects.

The Schottky barriers help spin injection and detection by overcoming the resistance mismatch problem.[29] This infamous resistance mismatch problem was first pointed out in the work of Schmidt et al [30], which showed that the resistances of the ferromagnet contacts ( $R_{fm}$ ) and the semiconductor spacer layer ( $R_{sc}$ ) must be matched in order to get a significant spin polarization in the semiconductor spacer layer. Unfortunately,  $R_{fm}/R_{sc}$  is usually of the order of  $10^{-4}$  since the spacer is a semiconductor and the ferromagnet is a metal. One way to overcome this problem is to use semiconductor ferromagnets instead of metallic ferromagnets, which is problematic since there are few semiconducting ferromagnets. Later Rashba pointed out that spin injection from ferromagnets to semiconductors can be significantly improved by placing a tunnel barrier between the two [29]. These barriers create a considerable difference in electrochemical potentials for spin-up and spin-down electrons, which aids efficient spin injection under the

condition of slow spin relaxation in the semiconductor spacer. The Schottky barriers, which are formed between Co-InSb and InSb-Ni, act as the tunnel barriers which improve the efficiency of spin injection and detection[31].

Through the point defect sites, electrons tunnel resonantly if their energy matches with those of the defect sites. Resonant tunneling is not occurring through the entire spacer layer, but instead only through the resonant energy levels of the localized defect sites.

Transport between two defect sites is not by normal tunneling, but by drift and spans a much longer distance. Therefore, some spin relaxation occurs between defects and this is the case where the “single subband transport” between two successive defects makes a difference regarding the amounts of spin relaxation that occurs. Single subband transport eliminates the DP relaxation and suppresses spin relaxation that occurs between successive defect sites.

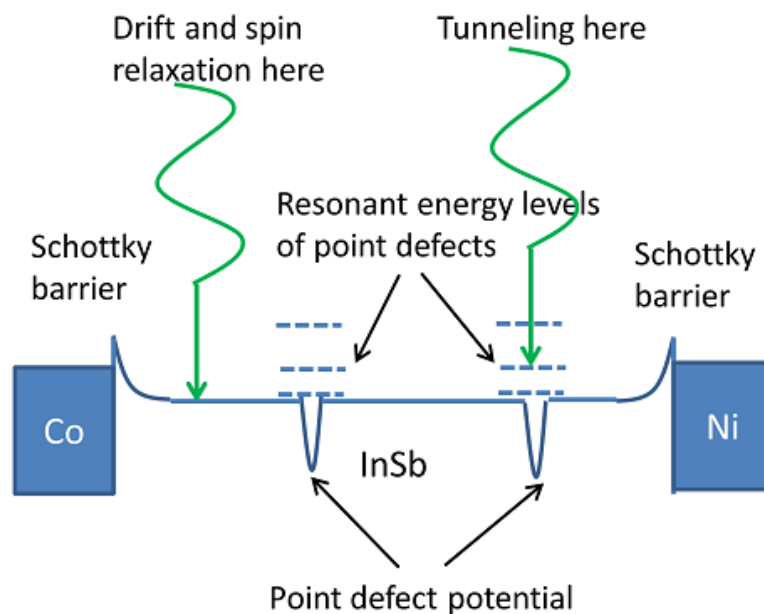


Figure 2-11: Transport model of an electron in metal semiconductor metal spin valve

## 2.6 SPIN POLARIZED CURRENT CONDUCTION MECHANISM IN SPACER LAYER:

So far, we have qualitatively discussed the role of spin relaxation length in spin polarized current. In this section, we will mathematically derive the relationship between the spin polarized current, spin injection and detection efficiency of the contacts and spin relaxation length. This relationship will also be helpful for the topics in chapter 3, where we will discuss the contrast between the dark current and current under IR light.

The spacer of a nanowire spin valve, which is sandwiched between two magnetic contacts, transporting spin polarized electrons from the left contact to the right contact as shown in the figure 2-12. It is assumed that the contacts are in the anti-parallel configuration. The left contact is polarized to the right and hence the majority spins in the left contact are polarized to the right. The opposite is true for the right contact.

Let the spin injection efficiency of the left contact is  $\eta_1$  and the spin detection efficiency of the right contact is  $\eta_2$ . There are four channels that contribute to the current.



Figure 2-12: Current conduction in a nanowire spin valve

1. The majority spins injected by the left contact flip and exit through the majority band of the right contact. The probability of flipping is  $(1 - e^{-\frac{L}{L_S}})$  where  $L$  is the separation between the contacts and  $L_S$  is the spin relaxation length. This channel contributed to the



current with a probability  $\frac{1+\eta_1}{2} (1 - e^{\frac{-L}{L_S}}) \frac{1+\eta_2}{2}$ . Here the probability of the left contact injecting a majority spin is  $\frac{1+\eta_1}{2}$  and the probability of the right contact transmitting through the majority band is  $\frac{1+\eta_2}{2}$ .

2. The majority spins injected by the left contact do not flip and exit through the minority band of the right contact. This channel contributes to the current with a probability of

$$\frac{1+\eta_1}{2} (e^{\frac{-L}{L_S}}) \frac{1-\eta_2}{2}.$$

3. The minority spins injected by the left contact do not flip and exit through the majority band of the right contact. This channel contributes to the current with a probability of

$$\frac{1-\eta_1}{2} (e^{\frac{-L}{L_S}}) \frac{1+\eta_2}{2}.$$

4. The minority spins injected by the left contact flip and exit through the minority band of the right contact. This channel contributes to the current with a probability of  $\frac{1-\eta_1}{2} (1 -$

$$e^{\frac{-L}{L_S}}) \frac{1-\eta_2}{2}.$$

Adding up all these contributions, we get that the channel current is proportional to-

$$\begin{aligned} I_{SD} &\propto \frac{1+\eta_1}{2} (1 - e^{\frac{-L}{L_S}}) \frac{1+\eta_2}{2} + \frac{1+\eta_1}{2} (e^{\frac{-L}{L_S}}) \frac{1-\eta_2}{2} + \frac{1-\eta_1}{2} (e^{\frac{-L}{L_S}}) \frac{1+\eta_2}{2} + \frac{1-\eta_1}{2} (1 - e^{\frac{-L}{L_S}}) \frac{1-\eta_2}{2} \\ &= \frac{1 - \eta_1\eta_2}{2} + \eta_1\eta_2 e^{\frac{-L}{L_S}} = \frac{1 - \eta_1\eta_2 + 2\eta_1\eta_2 e^{\frac{-L}{L_S}}}{2} \dots \dots \dots (2.5) \end{aligned}$$

### 3 MODULATION OF D'YAKONOV PEREL' MECHANISM

---

The ability to modulate the spin relaxation rate in a device with an external agent can open up several opportunities.[32] In this chapter, the idea of a novel spintronic infrared (IR) detector is highlighted which is backed by preliminary experimental evidence.

#### 3.1 MANIPULATION OF SPIN RELAXATION WITH IR LIGHT

Consider the spin valve structure shown in figure 3-1. One ferromagnetic contact is Co and the other is Ni. Let us assume that their magnetizations are antiparallel (the case when the contact magnetizations are parallel is analogous and hence not repeated here). The left contact FM1 injects electrons whose spins are polarized to the right. If there is no spin relaxation in the InSb spacer layer (Sp), then the spins that arrive at the right contact FM2 are polarized to the right and are blocked by the right contact because the latter is magnetized to the left. Therefore, little or no electron flow occurs and the device resistance is high.



FM = ferromagnet

Sp = spacer

Figure 3-1: A nanowire spin valve whose two ferromagnetic contacts have opposite signs of tunneling spin polarization

Next, we illuminate the device with IR light that induces transitions of electrons from the lowest to higher subbands in the InSb nanowires. This revives (or at least increases) the DP relaxation. Therefore, some of the electrons injected by FM1 flip their spins within the spacer layer and when these electrons arrive at the right contact FM2, their spins are parallel to the right contact's magnetization and hence they transmit, resulting in higher current through the spin valve (lower resistance). Therefore, this device acts like a photodetector. The dark conductance is lower than the conductance under illumination, which allows photodetection. The reader can surmise easily that if the contacts have parallel magnetizations, then we will obtain an "inverse photodetector", i.e. the device conductance will be lower under illumination than in the dark. In either case, photodetection is realized.

We assume that IR light only induces intra-band transitions in the conduction band of the spin valve's spacer layer and not interband transitions from the valence to the conduction band which would have changed carrier concentration. This assumption would be particularly true for wide gap semiconductor spacers where the bandgap vastly exceeds the IR photon energy. Also we assume that, current in the spacer layer is mostly due to drift, not diffusion. In that case, the current expression would be:

$$I = \frac{ev_d n_l}{4} [1 + \zeta_1 \zeta_2 - 2\zeta_1 \zeta_2 e^{-\frac{L}{L_s}}] \dots \dots \dots (3.1)$$

Where  $e$  is the electron charge,  $v_d$  is the drift velocity of electrons,  $n_l$  is the linear electron concentration in the spacer layer,  $L$  is the length of the spacer layer,  $\zeta_1$  is the spin injection efficiency at the injecting (left) contact,  $\zeta_2$  is the spin detection efficiency at the detecting (right) contact and  $L_s$  is the spin relaxation length in the spacer layer, ensemble averaged over electron velocity.

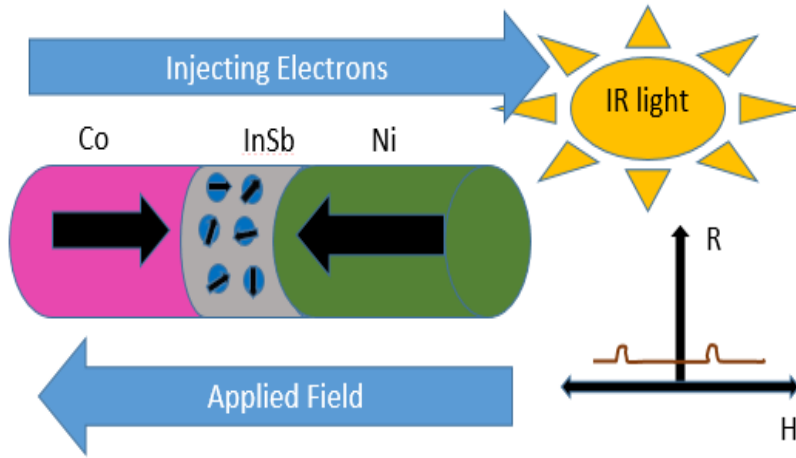


Figure 3-2 : Spins become randomized due to applied IR illumination. The magnetoresistance peaks also get muted, due to the absence of spin dependent transport.

In deriving the above equations, two assumptions have been made. First, even in single subband transport (when DP relaxation is absent), spin orbit interaction will make the spins precess as they travel, but the angle  $\theta$ , by which they precess is same for all since they are travelling over the same distance  $L$  with the same drift velocity  $v_d$ . For our system, we have assumed a very small  $L$ , hence  $\theta$  is also very small and hence we neglect this effect.

Assuming  $\zeta_1$  and  $\zeta_2$  is independent of IR light, the light to dark current contrast ratio will be,

$$\text{Contrast ratio} = \frac{I_{\text{Light}}}{I_{\text{dark}}} = \frac{1 + \zeta_1 \zeta_2 - 2\zeta_1 \zeta_2 e^{-\frac{L}{L_l}}}{1 + \zeta_1 \zeta_2 - 2\zeta_1 \zeta_2 e^{-\frac{L}{L_d}}} \dots \dots \dots (3.2)$$

where  $L_l$  and  $L_d$  are spin relaxation lengths under IR illumination and in the dark, respectively.

In the event  $L_l, L_d \gg L$ , the above expression simplifies to

$$\text{Contrast ratio} = \frac{I_{\text{Light}}}{I_{\text{dark}}} \approx \frac{1 + \zeta_1 \zeta_2 + 2\zeta_1 \zeta_2 \left(\frac{L}{L_l}\right)}{1 + \zeta_1 \zeta_2 + 2\zeta_1 \zeta_2 \left(\frac{L}{L_d}\right)} \dots \dots \dots (3.3)$$

$$\approx \frac{L_d}{L_l} \text{ if } \zeta_1 \approx \zeta_2 \approx 1 \dots \dots \dots (3.4)$$

Ideally,  $L_d$  will be infinite in a strictly one-dimensional wire since DP relaxation is absent and most other spin relaxation mechanisms are very weak. Therefore, this effect could be exploited to implement a photodetector with extremely high light-to-dark contrast ratio.

### 3.2 EXPERIMENTAL SETUP

The experimental setup is very close to the one we used for spin transport measurement. In this experiment, we have made spin valves by depositing 3 layers of materials (Co, InSb, and Ni respectively). Here Co has been deposited for a very small duration (30 seconds of deposition) whereas Ni has been deposited for a long time (4 minutes). Ni will have a long cylindrical shape, and due to shape anisotropy, its easy axis of magnetization will also be along the cylindrical axis. On the other hand, due to the short deposition time, Co layers are very short, and do not necessarily have the cylindrical shape. Most probably they are shaped like a circular disk where the easy axis is perpendicular to the cylindrical axis (hence perpendicular to the easy axis of Ni contacts) as shown in figure 3-3. Of course, at high enough magnetic field, the magnetization of Co contacts will rotate along the field and hence along the nanowire axis. For each nanocontact, this alignment will be happen abruptly when the magnetostatic energy due to the applied magnetic field equals the shape anisotropy energy. Due to the large contact area of our samples, almost  $3 \cdot 10^9$  nanowires are contacted in parallel. If the variation of shape anisotropy energy barrier among all the Co nanocontacts is small, then all the contacts will switch their

magnetization almost at the same magnetic field and the magnetizations will be aligned in a parallel direction with Ni. At that field, we should see a sudden jump of conductance. But if shape anisotropy among the nanowires varies a lot, the magnetizations of the Co nanocontacts will change direction at different magnetic fields (although each of them switches instantly). Hence we will see a gradual change in resistance. Again, due to inverse spin valve effect, the polarization of one of the contacts might get reversed which would cause an abrupt dip (as opposed to an abrupt jump) in the spin-valve's conductance at a threshold magnetic field. In fact, one of our sample did so, but the other one followed normal spin valve behavior.

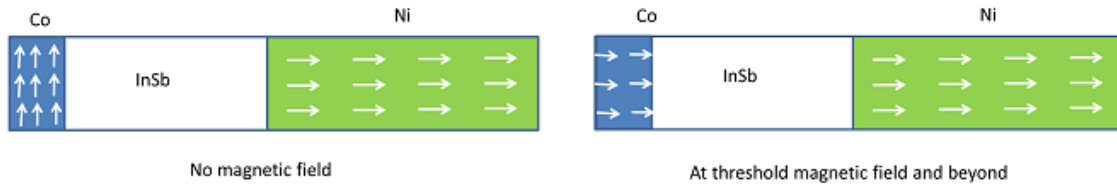


Figure 3-3: The magnetizations of the two contacts below and above the threshold magnetic field

### 3.3 IR SENSITIVITY OF MAGNETORESISTANCE:

In figure 3-4, we have measured the magnetoresistance of a sample both in dark and under infrared (IR) illumination. The magnetoresistance was measured with a magnetic field directed parallel to the axes of the wires. The lamp was kept far away from the sample to avoid heating effects and photocurrent generation. The resistance of the sample under illumination was monitored over time to see if there is a drift in resistance. Since, there was no drift, it can be concluded that, heat due to the IR lamp has no discernible effects on resistance.

When the magnetoresistance measurement was done in dark, we observed an abrupt jump in resistance by 2.5% when the magnetic field exceeds  $\pm 650$  Oe.

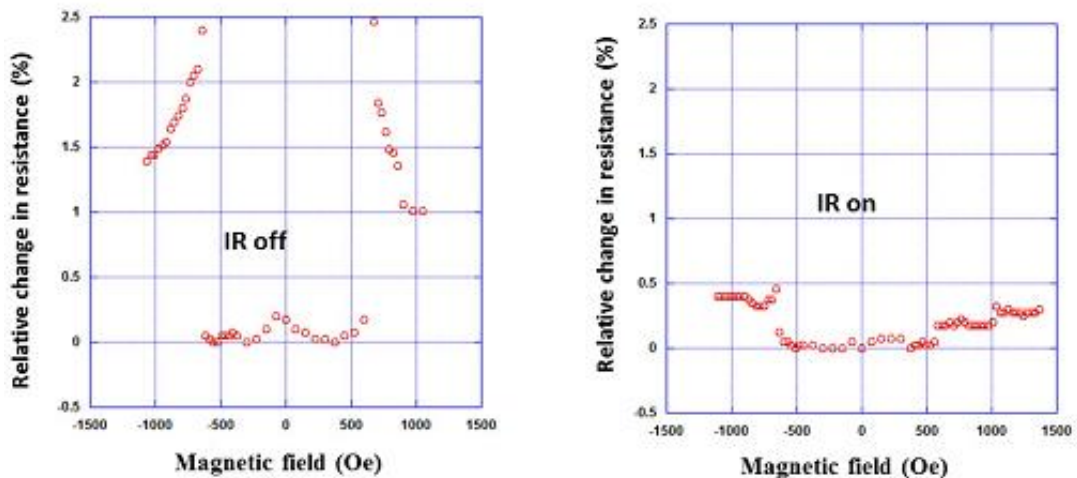


Figure 3-4: Room-temperature magnetoresistance of a Co-InSb-Ni nanowire spin-valve sample in the dark (above) and under illumination by an infrared lamp radiating in the wavelength range 2-5 $\mu$ m (below). The zero-field dark resistance was 4.2 ohms.

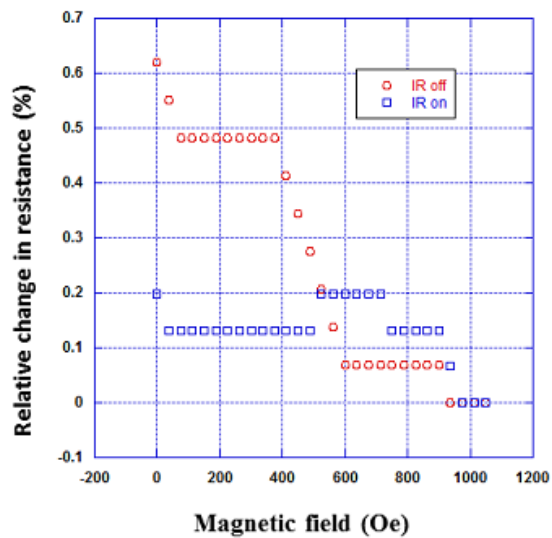


Figure 3-5: Room-temperature magnetoresistance of another Co-InSb-Ni nanowire spin-valve sample in the dark and under illumination by an infrared lamp radiating in the wavelength range 2-5  $\mu$ m. The zero-field dark resistance was 9.7 ohms.

Since the jump is reproducible, surely this is the threshold field when the magnetization of the Co aligns with that of Ni. Also the abrupt jump indicates that variation in the shape anisotropy energy among the nanowires is small. Since the resistance jumps instead of dipping, this sample exhibits the inverse spin valve effect, i.e. the resistance is higher when the contact magnetizations are mutually parallel.

Beyond the threshold field, the resistance drops with increasing field. This could be due to the fact that with increasing magnetic field, the energy separation between the subbands increases, hence inter subband scattering decreases. This is not a spin sensitive effect, but this phenomenon gives us the confidence that the abrupt jump is in fact due to spin polarized transport.

The same measurement was done under IR illumination. The same resistance jump around  $\pm 650 Oe$  is observed, but the change of resistance is only 0.4%, which is more than six times smaller than the previous case. This is only possible if IR light weakens the spin polarized transport. IR light excites the electrons to higher subbands, therefore creating multi subband transport. Multi subband transport revives the DP spin relaxation mechanism and spin relaxation rate increases, which makes spin relaxation length shorter. The shorter spin relaxation length decreases the spin polarized current and hence suppresses the step increase in the magnetoresistance in the threshold field.

A rough approximation of the spin relaxation length in the InSb spacer layers can be found using the modified Julliere formula for drift transport [19], [33] –

$$\frac{\Delta R}{R} = - \frac{2P_1P_2e^{-\frac{L}{L_s}}}{1-P_1P_2e^{-\frac{L}{L_s}}} \dots \dots \dots (3.5)$$



Where  $\frac{\Delta R}{R}$  is the relative change in the resistance at the step,  $P_1, P_2$  are the spin polarizations of the two contacts,  $L$  is the average length of the InSb layer and  $L_s$  is the average spin relaxation length. For these set of samples, from TEM observation, we have found  $L \approx 40 \text{ nm}$  (Figure 3-6). For Co, we have assumed  $P_1 = 0.1$  [20][34] (as Co nanocontacts are small) and for Ni, we have assumed  $P_2 = 0.33$  (each Ni nanocontact is of cylindrical shape, but the common contact area is about  $6 \text{ nm}^2$  and approximate bulk.) [35]. So using  $\frac{\Delta R}{R} = 2.5\%$ , we get  $L_s \approx 40 \text{ nm}$  in the dark and using  $\frac{\Delta R}{R} = 0.4\%$ , we get  $L_s \approx 14 \text{ nm}$  under illumination. Thus, the spin relaxation length decreases by 3 times under IR illumination.

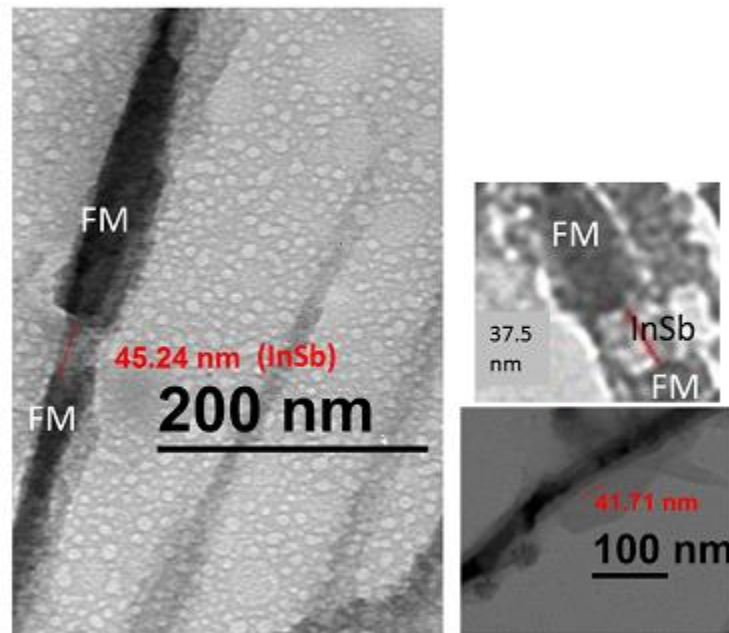


Figure 3-6: Bright field transmission electron micrograph of Co-InSb-Ni nanowire spin valves formed within anodic alumina pores of 50 nm diameter (FM=ferromagnet). The InSb spacer layer length varies from wire to wire because of the fabrication process, but the spread is not large and the average spacer layer length is  $\sim 40 \text{ nm}$ . In the TEM samples, the Co electrodeposition time was intentionally increased to 4 minutes in order to obtain a long Co section for sufficient contrast that will allow unambiguous determination of the InSb spacer layer's length. In the actual spin valves, the Co section is much shorter because the electrodeposition time was only 30 seconds.

It is reasonable to assume that  $P_1 = \zeta_1$  and  $P_2 = \zeta_2$ . Now using the following equation (derived from 3.5), where  $L_l$  is the spin relaxation length under illumination  $L_d$  is that in the dark,

$$\frac{R_d - R_l}{R_l} = 2\zeta_1\zeta_2 \frac{e^{-\frac{L}{L_d}} - e^{-\frac{L}{L_l}}}{1 + \zeta_1\zeta_2 - 2\zeta_1\zeta_2 e^{-\frac{L}{L_d}}} \dots \dots \dots (3.6)$$

where  $\zeta_1 = 0.1$ ,  $\zeta_2 = 0.33$ ,  $L=40nm$ ,  $L_d=40 nm$ , and  $L_l=14 nm$ , we estimate that the relative change of resistance should be 2% where  $R_d$  is the dark resistance,  $R_l$  is the resistance under illumination. Our experiments also show the relative change is 2%, showing excellent match between theory and experiment.

Figure 3.5 shows the magnetoresistance of another sample measured both in the dark and IR illumination. In the dark, the sample shows a gradual decrease in the range of 400-600 Oe. This tells us two things: (1) the shape anisotropy energy barriers among the Co nanocontacts vary a lot. (2) The decrement in resistance also tells us that, there has been no resonant tunneling rather it was the normal spin valve effect. The drop is 0.4%. Under illumination, there is no discernible change in resistance with increasing magnetic field (the random jumps of 0.1% changes show no symmetric trend). This result indicates that there has been no significant spin polarized transport because average spin relaxation length has become much shorter than the spacer length. Equation 3.6 shows that  $L_d=14nm$  for this sample, and unmeasurable under illumination.

The IR source is a broadband lamp and radiates in the wavelength range between 2 and 5  $\mu m$  corresponding to the photon energies between 9.4 kT and 24 kT, while the effective bandgap of the InSb layer is around 6.5 kT. The IR illumination hence induces both interband transition (valence to conduction band) and inter subband transition within the conduction band of InSb spacer layer. The resistance of the sample under zero magnetic field (when significant spin

polarized transport does not occur) however decreased by only 0.15% under illumination indicating that the interband transitions (which will increase the electron and hole concentration in conduction and valence band respectively, hence increasing the conductance) is not significant. The IR source is therefore also too weak to cause any significant intraband (or inter-subband) transitions, and yet spin relaxation length decreased by a factor of three under illumination. This is because even slight deviation from the single subband transport can increase the DP relaxation considerably. This is encouraging since it not only portends high detectivity, but also small noise equivalent power for photodetectors predicted on this effect.

If the spin polarization of the contacts can be improved and EY and other spin relaxation mechanisms can be suppressed by producing high mobility samples with weak hyperfine interactions, then this effect can be used to obtain very high light-to-dark contrast ratio. With 100% injection and detection efficiency, this contrast ratio ( $I_{\text{light}}/I_{\text{dark}}$ ) will be infinite. Such a photo-detector will also ideally have nearly zero dark current and hence almost zero standby power dissipation, making it very attractive. The experiments reported here lay the groundwork for such a device.

## **4 GIANT MAGNETO-CONDUCTANCE DUE TO MAGNETIC FIELD ASSISTED MODULATION OF LOCAL ELECTRON CONCENTRATION:**

---

In this section, we will discuss a new effect that has been observed in single (or few) nanowire structures with non-magnetic contacts. The magnetoresistance of these structures can be changed by five orders of magnitude with a magnetic flux density of  $\sim 100$  mT, resulting in a super-giant magnetoresistance sensor.

Consider a parallel array of Cu nanowires between two Au contacts as shown in figure 4-1.a. Since Cu oxidizes in the ambient, the nanowires will have an ultrathin  $\text{Cu}_2\text{O}$  or  $\text{CuO}$  coating, which will be interposed between the Au contacts and the Cu conductor. The bandgap of this coating is between 1.6 and 2.54 eV[36]. Hence, it will result in a potential barrier of several  $kT$  between the Cu and Au ( $kT$  is the room temperature thermal energy).

When a potential difference  $V$  is imposed between the contacts to induce current flow, the energy band diagram in the direction of current flow (along the wire) will appear as shown in figure 4-1.b. Current flows by electrons either tunneling through, or thermionically emitting over the barriers, or by both mechanisms. The magnitude of the resistance will depend exponentially on the barrier heights (for thermionic emission)[26] or the square-root of the barrier heights (for tunneling)[26]. Any modulation of the barrier heights will therefore cause a large change in a wire's resistance.

Consider now the situation when a magnetic field is applied transverse to the direction of current flow. The resulting Lorentz force will divert electrons toward one edge of the wire, resulting in electron accumulation at that edge and depletion at the opposite edge as shown in figure 4-2.a.

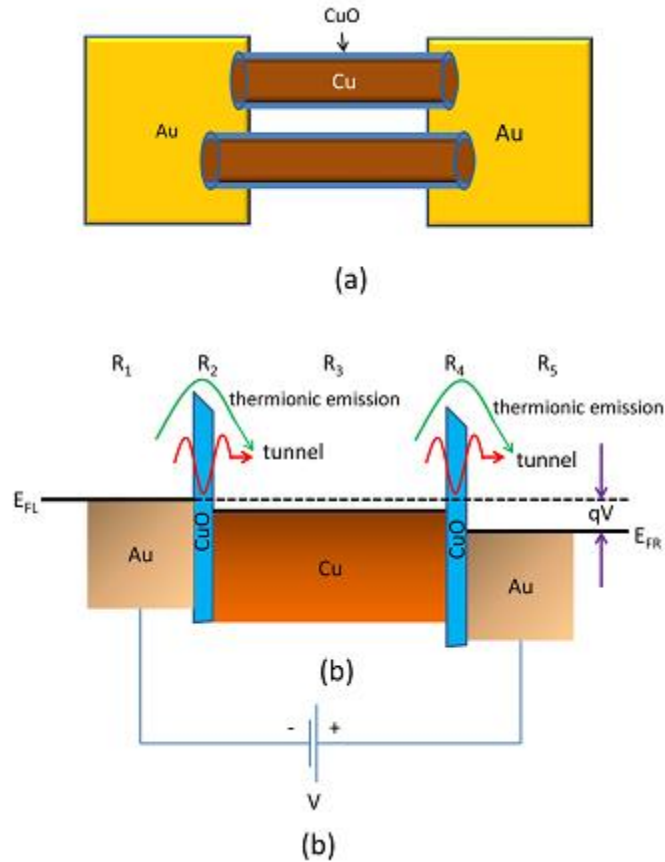


Figure 4-1: [Color online] (a) An array of Cu wires with a thin oxide coating captured between two Au contact pads.

(b) The potential energy diagram in the direction of current flow under an applied bias  $V$ . The Fermi levels in the left and right contacts are denoted by  $E_{FL}$  and  $E_{FR}$ , respectively, while  $q$  is the electron charge. The resistance of the structure can be thought of as being composed of five resistors in series – the resistance  $R_1$  due to the left Au contact, the resistance  $R_2$  due to the left tunnel barrier, the resistance  $R_3$  due to the Cu wire, the resistance  $R_4$  due to the right tunnel barrier and the resistance  $R_5$  due to the right Au contact. The dominant resistances are  $R_2$  and  $R_4$ .

Consequently, the energy band diagram at the two edges will look like in figure 4-2.b, where the barriers are shorter at the accumulated edge and taller at the depleted edge. Thus, electrons can tunnel (or thermionically emit) much more easily at the top edge than at the bottom edge.

As shown in figure 4-2.b, the resistance of the structure can be thought of as being composed of five resistors in series – the resistance  $R_1$  due to the left Au contact, the resistance  $R_2$  due to the

left barriers (at the accumulated and depleted edges), the resistance  $R_3$  due to the Cu wire, the resistance  $R_4$  due to the right barriers, and the resistance  $R_5$  due to the right Au contact. The dominant resistances are  $R_2$  and  $R_4$  (since the other resistances are of metallic structures) and these two are modulated by the magnetic field.

Let us carry out a qualitative analysis of how the resistance between the two contacts can change in a magnetic field due to barrier height modulation at the top and bottom edges caused by the deflection of the electron trajectories. Because the analysis is “qualitative”, we will view each of the resistances  $R_2$  and  $R_4$  as being roughly due to two parallel paths – one along the top edge and the other along the bottom. We will call the resistances of the two barriers at the top edge  $R_\alpha$  and  $R_\beta$ , while calling the resistances of the two barriers at the bottom edge  $R_\gamma$  and  $R_\delta$  (see figure 4-2.b). The resistance of the structure can therefore be written as:

$$\begin{aligned}
 R &= R_1 + (R_\alpha \parallel R_\gamma) + R_3 + (R_\beta \parallel R_\delta) + R_5 \\
 &\approx (R_\alpha \parallel R_\gamma) + (R_\beta \parallel R_\delta) \\
 &= \frac{1}{\frac{1}{R_\alpha} + \frac{1}{R_\gamma}} + \frac{1}{\frac{1}{R_\beta} + \frac{1}{R_\delta}} \dots \dots \dots (4.1)
 \end{aligned}$$

The resistances  $R_\alpha$ ,  $R_\beta$ ,  $R_\gamma$  and  $R_\delta$  are determined by tunneling and/or thermionic emission. Let us consider the tunneling case first. Within the WKB approximation, the tunneling transmission probability of an electron impinging on a barrier with energy  $E$  is [26]

$$|T(E)| = \exp \left[ - \int_{x_1}^{x_2} dx \sqrt{2m^* \frac{(E_c(x) - E)}{\hbar^2}} \right] \dots \dots \dots (4.2)$$

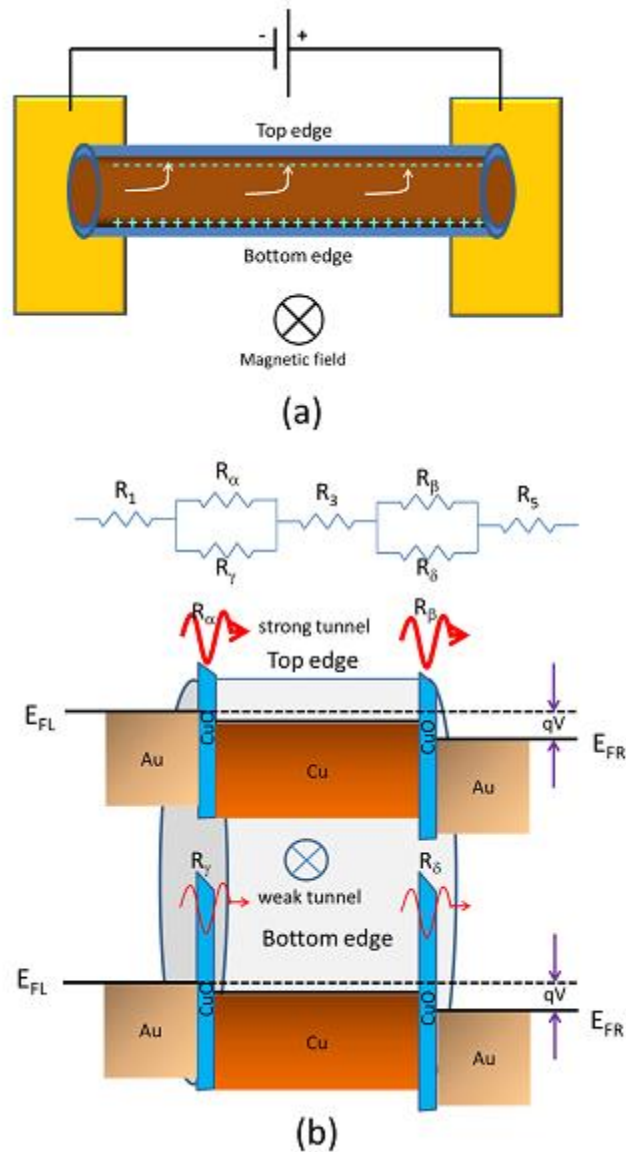


Figure 4-2 [Color online] (a) When a magnetic field is applied transverse to the direction of current flow, the resulting Lorentz force deflects electrons towards one edge, causing accumulation at one edge (in this case the top edge) and depletion at the opposite edge (in this case the bottom edge). (b) Accumulation shifts the Fermi level upwards with respect to the conduction band edge in a metal while depletion shifts it downwards. Therefore the potential barriers become shorter at the accumulated (top) edge and taller at the depleted (bottom) edge. Electrons tunnel through (or thermionically emit over) the barriers much more easily at the top edge than at the bottom edge, making the resistances due to the barriers vastly different at the top and bottom.

where the x-axis is in the direction of current flow, the tunnel barrier extends from  $x = x_1$  to  $x = x_2$ , and  $E_c(x)$  is the spatially varying potential energy of the tunnel barrier. Similarly, within the Richardson model, the thermionic emission probability is inversely proportional to the exponential of the (spatially averaged) barrier height at any given temperature. [26] Here, we will analyze the tunneling case. The reader can easily replicate the analysis for the thermionic emission case.

In the tunneling case, the resistance of any barrier is inversely proportional to the tunneling probability. Hence,

$$R_m \propto e^{\sqrt{\Delta_m/\Delta}} \dots \dots \dots (4.3)$$

Where  $R_m$  is the resistance and  $\Delta_m$  is the (spatially averaged) height of the m-th barrier, while  $\Delta$  is a constant.

Thus, we obtain that in the absence of any magnetic field, the resistance is [from Equations (4.1) and (4.3)]

$$R_{B=0} \propto \left[ \frac{1}{e^{-\sqrt{\Delta_\alpha/\Delta}} + e^{-\sqrt{\Delta_\gamma/\Delta}}} + \frac{1}{e^{-\sqrt{\Delta_\beta/\Delta}} + e^{-\sqrt{\Delta_\delta/\Delta}}} \right]$$

$$\propto e^{\sqrt{\Delta_1/\Delta}} \frac{1}{\cosh(\Omega_1)} + e^{\sqrt{\Delta_2/\Delta}} \frac{1}{\cosh(\Omega_2)} \dots \dots \dots (4.4)$$

Where  $\Delta_1 = \frac{\Delta_\alpha + \Delta_\gamma}{2}$ ,  $\Delta_2 = \frac{\Delta_\beta + \Delta_\delta}{2}$ ,  $\Omega_1 \approx \frac{\Delta_\alpha - \Delta_\gamma}{4\sqrt{\Delta_1\Delta}}$  and  $\Omega_2 \approx \frac{\Delta_\beta - \Delta_\delta}{4\sqrt{\Delta_2\Delta}}$

In the presence of the magnetic field, the tunnel barrier heights decrease by  $\epsilon_\alpha$  and  $\epsilon_\beta$  at the top edge, while increasing by  $\epsilon_\gamma$  and  $\epsilon_\delta$  at the bottom edge ( $\epsilon_\alpha, \epsilon_\beta, \epsilon_\gamma, \epsilon_\delta > 0$ ). Therefore,



$$R_{B \neq 0} \propto e^{\sqrt{\Delta'_1/\Delta}} \frac{1}{\cosh(\Omega'_1)} + e^{\sqrt{\Delta'_2/\Delta}} \frac{1}{\cosh(\Omega'_2)} \dots \dots \dots (4.5)$$

Where

$$\Delta'_1 = \Delta_1 + (\epsilon_\gamma - \epsilon_\alpha)$$

$$\Delta'_2 = \Delta_2 + (\epsilon_\beta - \epsilon_\delta)$$

$$\Omega'_1 = \Omega_1 - (\epsilon_\gamma + \epsilon_\alpha) / \sqrt{4\Delta'_1\Delta} = \Omega_1 - \omega_1$$

$$\Omega'_2 = \Omega_2 - (\epsilon_\beta + \epsilon_\delta) / \sqrt{4\Delta'_2\Delta} = \Omega_2 - \omega_2 \dots \dots \dots (4.6)$$

The quantities  $\omega_1$  and  $\omega_2$  depend on the magnetic field and are positive. From Equations (4.4) - (4.6), we obtain that-

$$R_{B \neq 0} - R_{B=0} \propto \left[ e^{\sqrt{\Delta'_1/\Delta}} \frac{1}{\cosh(\Omega'_1)} - e^{\sqrt{\Delta_1/\Delta}} \frac{1}{\cosh(\Omega_1)} + e^{\sqrt{\Delta'_2/\Delta}} \frac{1}{\cosh(\Omega'_2)} - e^{\sqrt{\Delta_2/\Delta}} \frac{1}{\cosh(\Omega_2)} \right] \dots \dots \dots (4.7)$$

It is interesting to note that if the shrinkage in the barrier height at the top edge is roughly equal to the expansion in the barrier height at the bottom edge, i.e.  $\epsilon_\alpha \approx \epsilon_\gamma$  and  $\epsilon_\beta \approx \epsilon_\delta$ , then  $\Delta_1 \approx \Delta'_1$  and  $\Delta_2 \approx \Delta'_2$ . In that case, given that  $\Omega_1 \approx \Omega_2 \approx 0$ ,

$$R_{B \neq 0} - R_{B=0} \propto \left\{ e^{\sqrt{\Delta'_1/\Delta}} \left[ \frac{1}{\cosh(\Omega_1 - \omega_1)} - \frac{1}{\cosh(\Omega_1)} \right] + e^{\sqrt{\Delta'_2/\Delta}} \left[ \frac{1}{\cosh(\Omega_2 - \omega_2)} - \frac{1}{\cosh(\Omega_2)} \right] \right\} < 0 \dots \dots \dots (4.8)$$

In this case, the resistance of the structure will always decrease in a magnetic field resulting in negative magnetoresistance. A similar analysis (algebraically easier) can be carried out for the case of thermionic emission, and the conclusion will be similar.

## **4.1 EXPERIMENTAL SETUP:**

In this section, the sample growth mechanism and measurement setup will be discussed.

### **4.1.1 Sample Growth and Characterization:**

The alumina template is grown as discussed earlier in section 2.1. Cu is electrodeposited selectively within the nanopores using a solution of 20gm of  $\text{CuSO}_4$ , 7 gm of boric acid in 1 liter of solution. After depositing the nanorods (figure 4-3.e), the alumina is dissolved using hot Chromic/Phosphoric acid, so that the Cu nanorods are standing vertically on top of Al substrate (figure 4-3.f).[37], [38]. The samples were then ultrasonicated in ethanol to release the wires from the aluminum foil, forming a suspension of Cu nanowires (50 nm diameter and varying length; average length  $\sim 1 \mu\text{m}$ ) in ethanol. Figure 4-4 and figure 4-5, respectively show the SEM images of Cu nanorods and their EDS spectra.

### **4.1.2 Dielectrophoresis:**

The Cu nanowires in the ethanol suspension were captured across Au contact pads on silicon chips using dielectrophoresis [39]–[41]. This involved the following steps. Electron beam lithography was used to create patterns in poly-methyl methacrylate (PMMA) based polymeric resists, which were spin-coated on silicon chips.

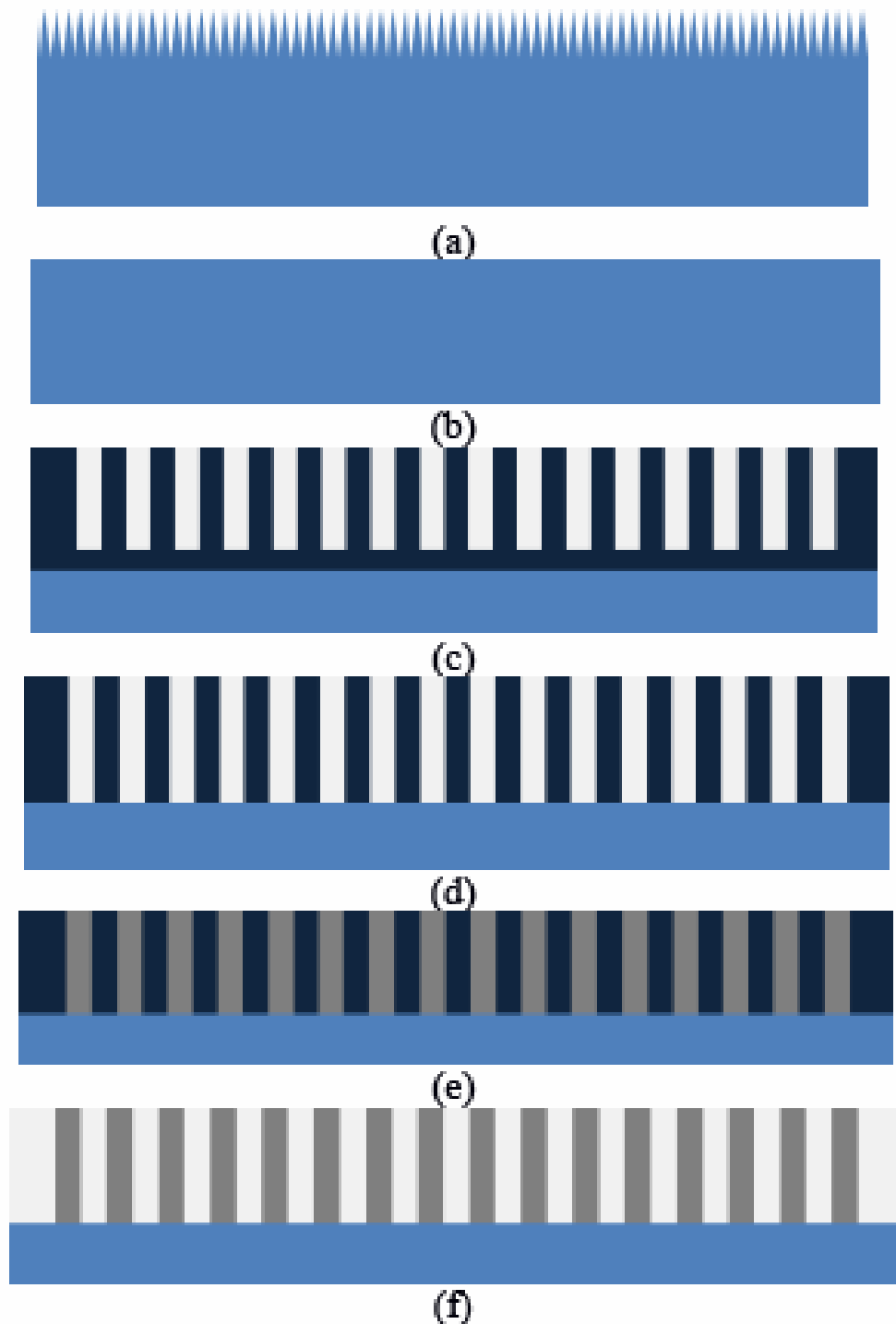


Figure 4-3: (a) 100  $\mu\text{m}$  thick rough Al foil. (b) Flat surface after electropolishing. (c) Porous Al<sub>2</sub>O<sub>3</sub> on top of Al foil. (d) Bottom barrier layer is removed using 5% Phosphoric acid. (e) Pores are filled with Cu using proper electrolyte and DC electrodeposition. (f) Alumina (Al<sub>2</sub>O<sub>3</sub>) layer is removed using Chromic-Phosphoric acid leaving behind free-standing nanorods.

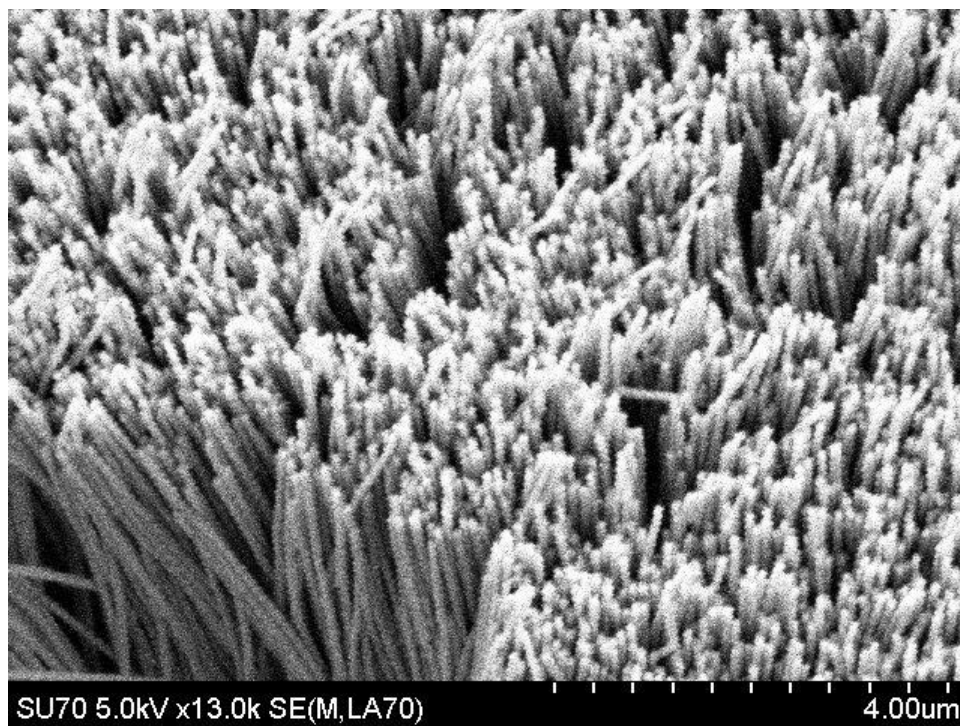


Figure 4-4: SEM image of free standing Cu nanorods

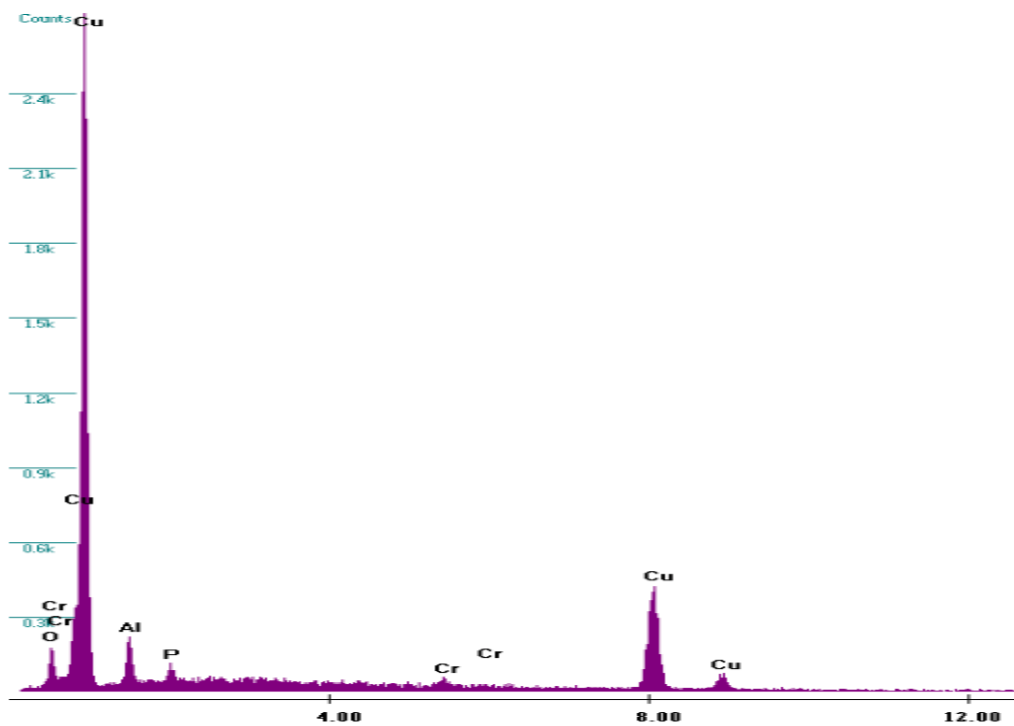


Figure 4-5: EDS spectrum of Cu nanorods on Al substrate, after Alumina is dissolved with hot Chromic/Phosphoric acid.

An 85-nm thick Au film (with a Cr adhesion layer) was deposited on the resist-patterned surface and metal lift-off was performed to create spatially separated nanoelectrode pairs on the chips. Next, the nanowire containing ethanol suspension was pipetted on to the surface of the silicon chip patterned with the Au nanoelectrodes, while applying an AC bias across the nanoelectrodes. This polarized the Cu nanowires in the suspension and exerted a dielectrophoretic (DEP) force that caused them to be captured across the nanoelectrodes. By tuning the excitation voltage (4V, peak-to-peak) and its frequency (1 KHz) over a given deposition period (4 minutes), the DEP region of influence was controlled to extend over suspension volumes that present single or a few nanowires. This resulted in an array of devices on the chip with a single or a few nanowires assembled across the Au nano-electrodes. From these assembled device arrays, single (or few) nanowire assembly locations were selected for further testing. A scanning electron microscope image of a representative device location with two assembled nanowires is shown in figure 4-6.

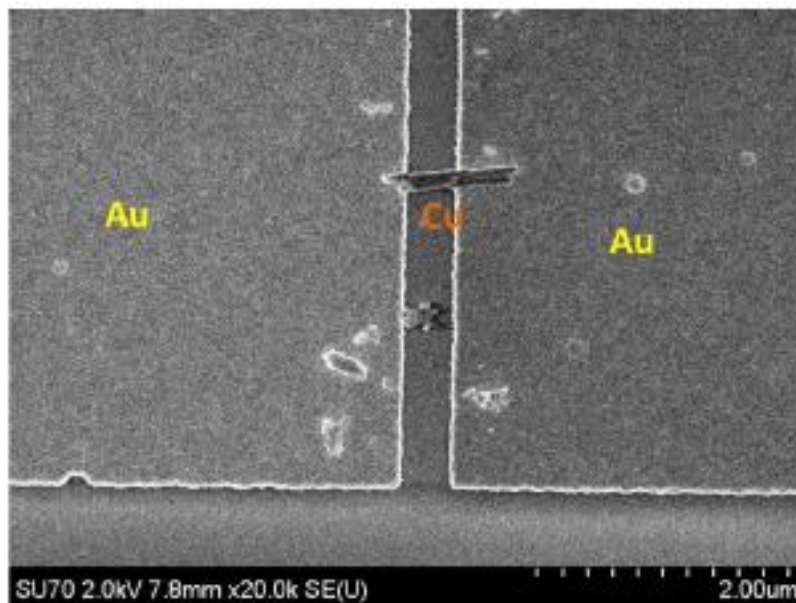


Figure 4-6: Scanning electron micrograph of two Cu nanowires captured between two Au contact pads.

### **4.1.3 Measurement setup:**

The I-V measurement is carried out with a HP 4156B semiconductor parameter analyzer under different magnetic fields. The magnetic field is applied by Neodymium (NdFeB) disk magnets.

## **4.2 I-V CHARACTERISTIC WITH RESPECT TO MAGNETIC FIELD:**

The characteristics in figure 4-7.a are expectedly non-linear because of the tunneling through, and/or thermionic emission over the barriers. The current at a given voltage increases with increasing magnetic field, resulting in a negative magnetoresistance (or positive magnetoconductance). The conductance at a fixed voltage of 7 V is plotted as a function of magnetic field in figure 4-7.b. In our set up, the maximum magnetic field we can apply is 75 mT.

In figure 4-8-a, we show the current-voltage plots for a fixed magnetic field strength of 39 mT, but for two anti-parallel directions of the field. There is a difference between the two cases since the electrons are deflected to opposite edges and the transport characteristics of the two edges are, expectedly, somewhat different. In this case, we have also plotted the current-voltage characteristic in log-linear scale in figure 4-8.b to show that the magnetoconductance is giant – the resistance can change by over five orders of magnitude in a magnetic field of 39 mT, resulting in a colossal magnetoresistance of 10,000,000% at that magnetic field and at a power supply voltage of few mV.

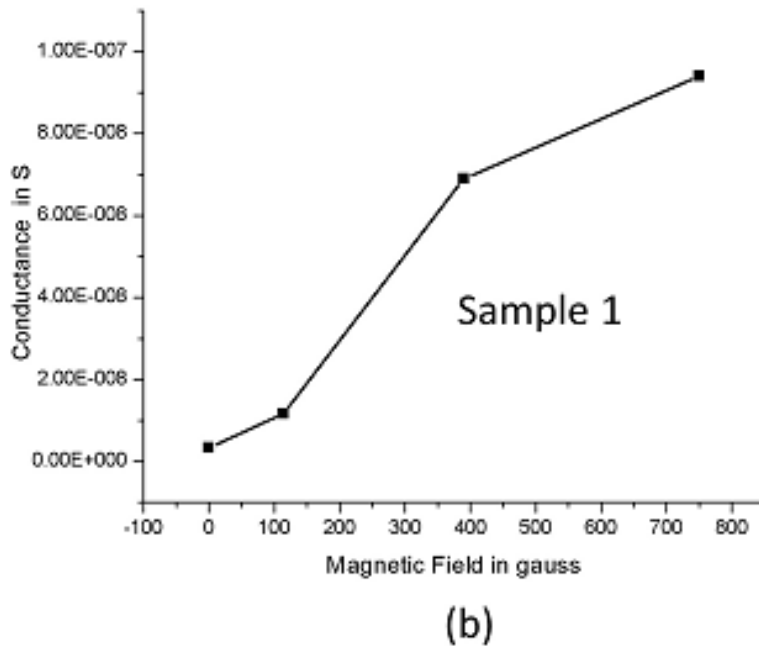
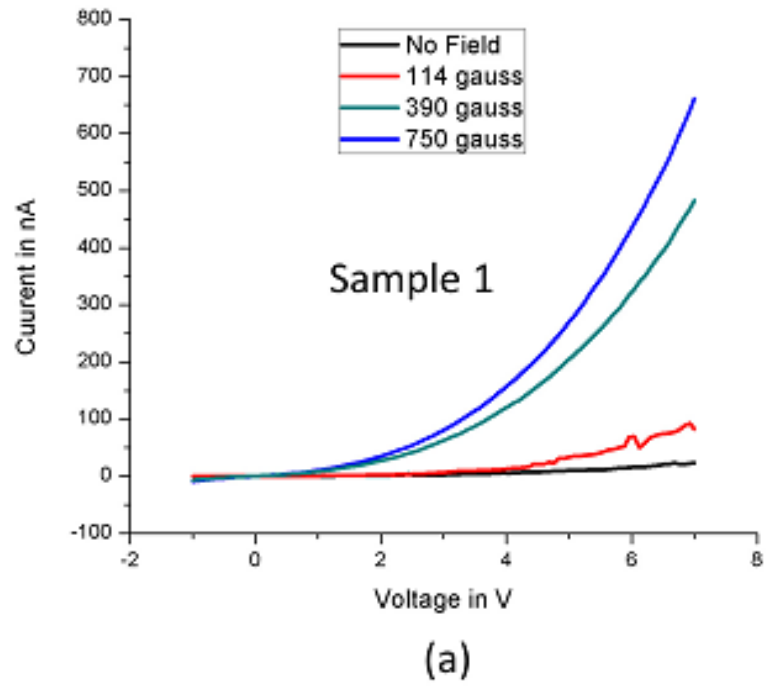
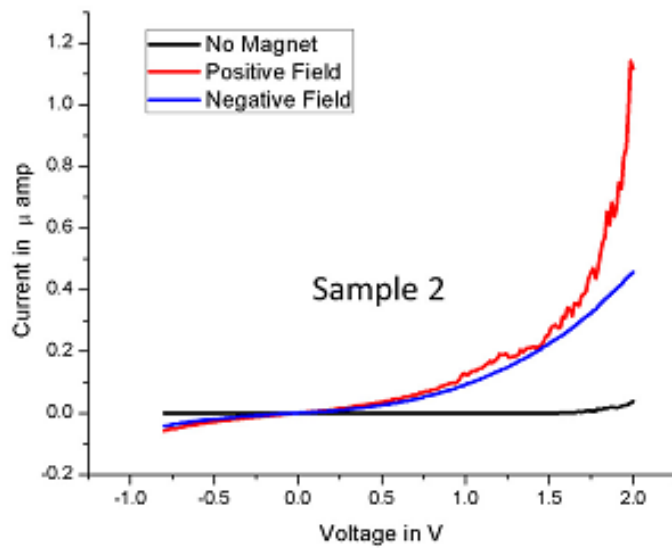
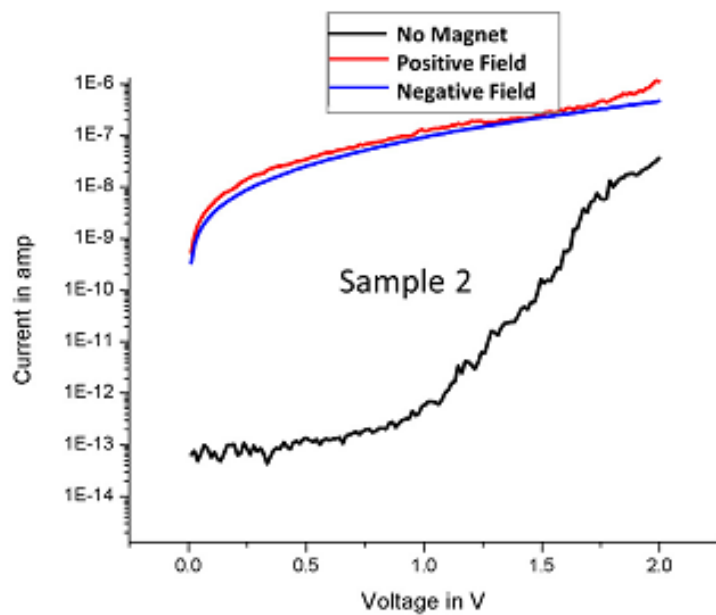


Figure 4-7: [Color online] (a) Current versus voltage characteristic of a sample plotted for zero and three different magnetic field strengths. (b) Magnetoconductance of the sample (conductance versus magnetic field) at a fixed voltage of 7 V.



(a)



(b)

Figure 4-8: [Color online] (a) Current versus voltage characteristics of a sample at zero magnetic field and at two opposite directions of a magnetic field of 39 mT. (b) The same current voltage characteristics plotted in a log-linear scale.



## 5 AMR SENSITIVITY WITH STRAIN

Anisotropic magnetoresistance (AMR) is a quantum mechanical phenomenon associated with spin-orbit coupling in a ferromagnet. When the magnetization of a magnet is collinear with the direction of current flow, the current experiences a higher resistance than when it is perpendicular to the direction of current flow. The resistivity relation is given by

$$\rho = \rho_0 + \rho_1 \cos^2 \theta \dots\dots\dots(5.1)$$

where  $\theta$  is the angle between the magnetization and the current.

The AMR effect always gives rise to a trough in the longitudinal magnetoresistance of a nanowire. To understand why this happens, consider a nanowire spin valve whose contacts are magnetized in one direction, along the wire axis, by a magnetic field as shown in the figure below. When the magnetic field is reversed, the magnetizations of the ferromagnetic contacts begin to rotate, which gradually increases the angle  $\theta$ . The resistance is minimized when  $\theta = 90^\circ$ , and then begins to increase again once  $\theta$  exceeds  $90^\circ$ . This will cause a trough in the magnetoresistance.

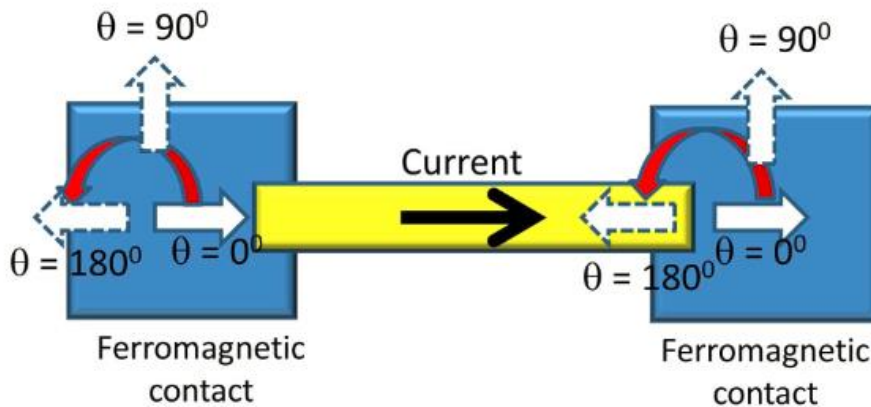


Figure 5-1: Switching of magnetization in a nanowire spin valve

## **5.1 COMPETING EFFECT OF AMR AND SPIN VALVE:**

The AMR effect co-exists with the spin valve effect. An interesting situation occurs when the spin-valve effect produces a magnetoresistance “peak”. Since the AMR always produces a “trough”, it will always decrease the height of the spin-valve peak. In the event when the AMR effect is weaker than the spin-valve effect, the latter will dominate but the peak height will be reduced. In the other event that the AMR effect is stronger than the spin valve effect, the former will dominate and we will no longer observe a peak, but instead observe a trough in the magnetoresistance since the AMR always produces a trough.

The AMR effect is very sensitive to strain. Consider a material like Co which has negative magnetostriction. A compressive strain will tend to align the spins in the direction of strain and this increases the AMR trough depth[42]. This provides us with a handle to modulate the AMR. We can generate compressive strain by heating the ferromagnet with an IR lamp. If the ferromagnet is delineated on a substrate whose thermal coefficient of expansion is smaller than that in the ferromagnet, then the ferromagnet will experience compressive strain. Therefore, the AMR effect will increase under heating. This becomes interesting when the spin valve effect dominates in the unstrained case and the AMR effect dominates under strain. In that case, we will see peak in the longitudinal magnetoresistance at room temperature, but a trough under heating. This is precisely what we have observed in a nanowire spin valve having a Cu spacer and Co ferromagnetic contacts.

## 5.2 EXPERIMENTAL SETUP

The sample growth, characterization and dielectrophoresis procedure are same as it was discussed earlier in the section 4.1. The measurement setup is the same as that discussed earlier in section 4.1.

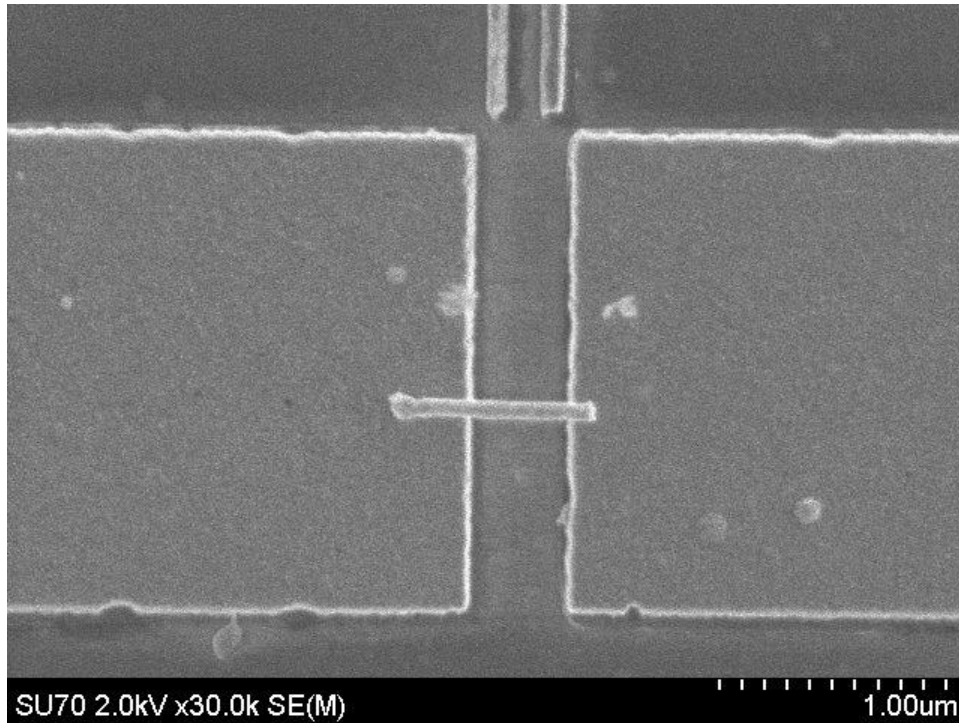
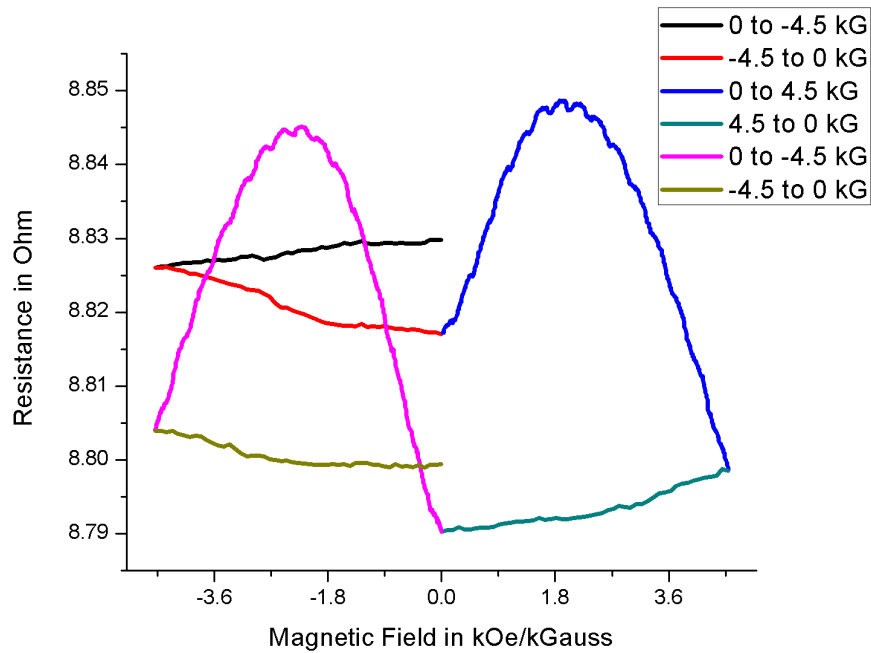


Figure 5-2: Cu nanowire between the Co contacts.

## 5.3 MAGNETORESISTANCE MEASUREMENT WITH AND WITHOUT IR LIGHT

The spin valve experiment gives us two distinct peaks which are shown in figure 5-3.



(a)

Figure 5-3: Magneto-resistance plot in Spin Valve measurement.

In figure 5-3, we show the magneto-resistance traces when the magnetic field is swept to high field values, then gradually reduced to zero, then reversed and swept to high negative fields and finally brought back to zero. We observe the tell-tale peaks corresponding to the normal spin valve effect. The peaks are very broad since the ferromagnetic contacts are large and consist of several domains, each with different orientation as shown in figure 5-4. Since different domains switch at different field strengths, it causes peak broadening.

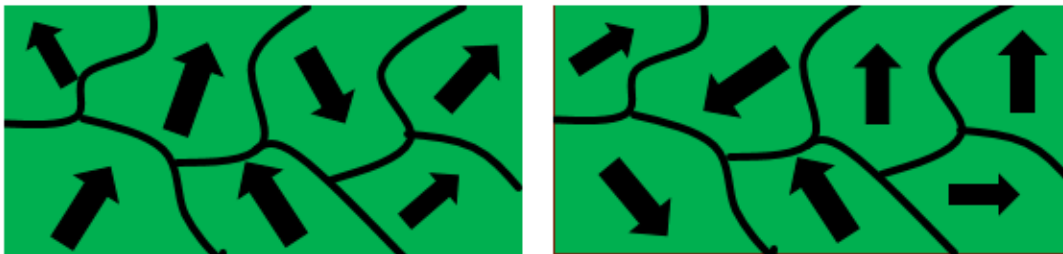
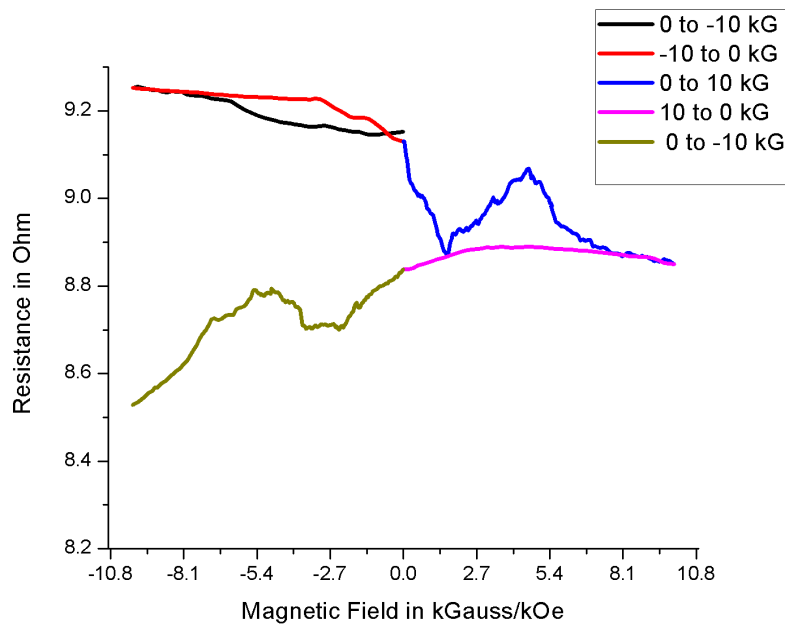


Figure 5-4: Multiple domains of Co pads where each of them has own favorable magnetic orientation.

When we shine IR light on the sample causing heating, the magnetoresistance (MR) curve looks like figure 5-5. Clearly, the peaks have been replaced with troughs, indicating that the AMR effect increased and ultimately overwhelmed the spin valve effect to cause the transition of the peaks into troughs. The ferromagnetic contacts are delineated on silicon whose thermal expansion coefficient is 5 times smaller than that of Co. Hence, Co expanded more under heating than Si, resulting in compressive strain within Co. That enhanced the AMR effect and caused the spin valve peak to be dominated by the AMR trough.



(a)

Figure 5-5: Magnetoresistance curve with IR light

If we plot the MR curves (with and without IR) in the same figure, as shown in figure 5-6, we see that in IR light (heating), AMR is dominating, while the spin valve (SV) is dominating in the dark (no heating).

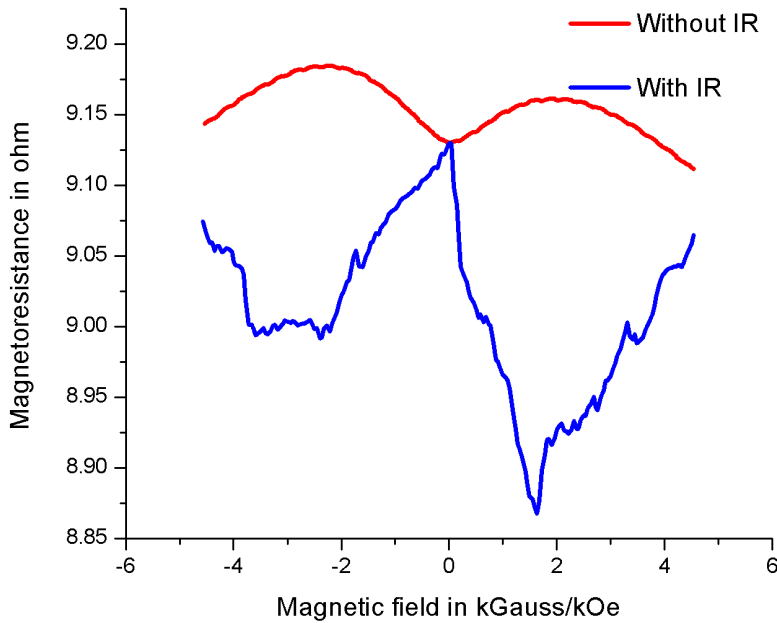


Figure 5-6: MR behavior in IR and without IR light.

The peak of SV and the trough of AMR are in the same position, which is confirmed by figure 5-6.

Since higher temperature results in higher strain, and higher strain results in higher magnetic order [42], the magnetoresistance jump should be higher if the sample is exposed to more heating. To test the hypothesis, we obtained the magnetoresistance traces with the IR lamp at two different distances from the sample, so that we can measure at two different temperatures. As expected, the AMR trough is much larger when the IR source is closer to the sample causing more heating and hence more strain in the sample. This experiment clearly demonstrates the effect of strain on AMR. With a thermocouple, we have measured the temperatures in the two cases – IR lamp at a distance and IR lamp in close proximity. In the first case, the temperature rise was 29.7 Celsius and in the latter case 34.1 Celsius.

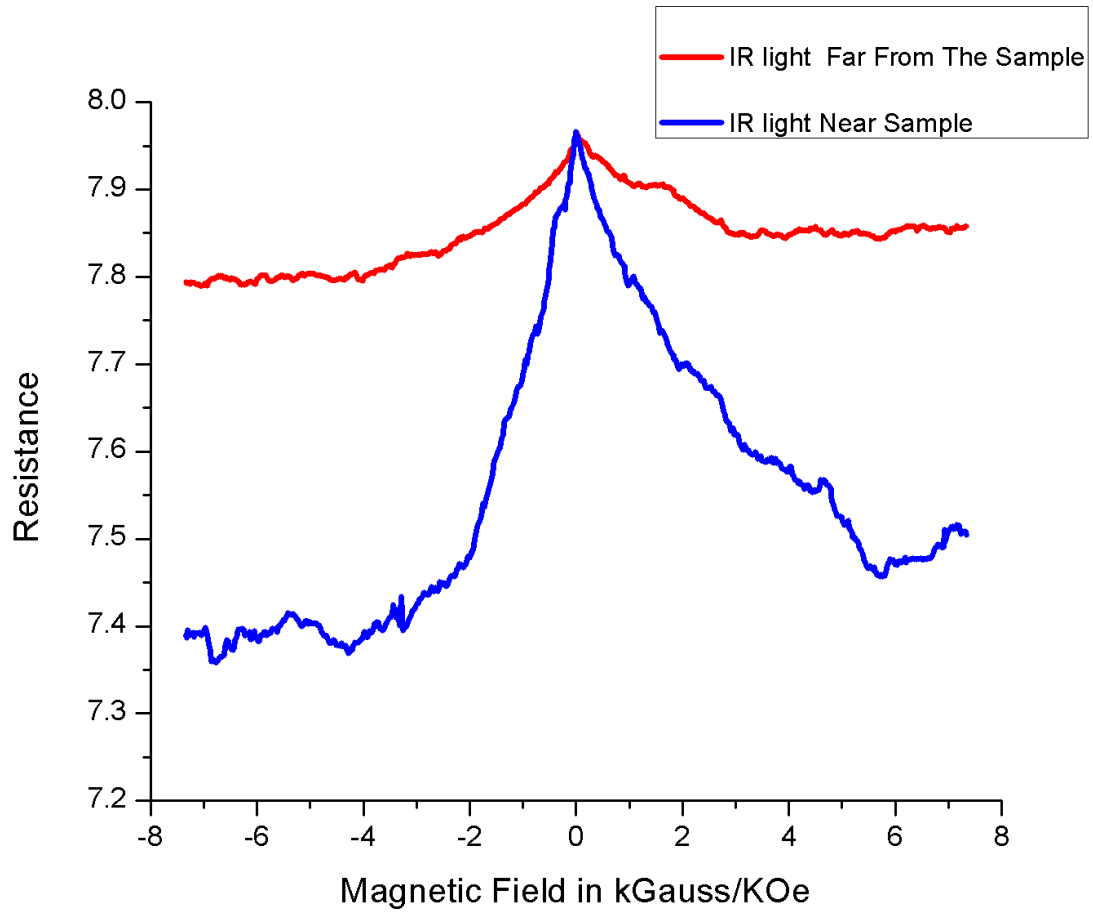


Figure 5-7: Magnetoresistance behavior with respect to the distance of IR light from the sample.

## 6 CONCLUSION:

---

In conclusion, we have studied spin transport in InSb nanowires and demonstrated both the spin valve and the Hanle effect at room temperature, thereby demonstrating spin injection, coherent spin transport and spin detection in a semiconductor at room temperature. The material InSb has a strong Rashba coefficient [30], which makes it an ideal candidate for the Datta-Das spin field effect transistor. This transistor requires a strictly one dimensional channel with a single subband occupied for the strongest effect [1]; hence, the demonstration of coherent spin transport in these single-subband occupied InSb nanowires – where the D'yakonov-Perel' spin relaxation has been suppressed – raises hopes for a room temperature device with significant conductance modulation.

We can also use this effect to implement a room-temperature IR detector with very high light-to-dark contrast ratio. Consider the situation when the spin injection/detection efficiencies approach 100%. From Equation (3), we get that the contrast ratio is  $L_d/L_l \approx L_{DP(s)}/L_{DP(m)} \rightarrow \infty$ , where  $L_{DP(s)}$  is the DP relaxation length in single-subband transport (ideally infinity) and  $L_{DP(m)}$  is the DP relaxation length in multi-subband transport (finite). Such a photodetector will also ideally have nearly zero dark current and hence almost zero standby power dissipation, making it very attractive. The experiments reported here lay the groundwork for such a device.

The demonstration of 10,000,000% super-giant magnetoresistance at only 390 gauss and a few mV bias across the sample could be used in all traditional applications of giant magnetoresistance, such as in magnetic read heads and magnetic field sensors. Demonstration of strain sensitive AMR sheds new light on our understanding of this intriguing quantum mechanical phenomenon.



## References

- [1] S. Bandyopadhyay and M. Cahay, *Introduction to Spintronics*. .
- [2] H. Masuda and M. Satoh, “Fabrication of Gold Nanodot Array Using Anodic Porous Alumina as an Evaporation Mask,” *Jpn. J. Appl. Phys.*, vol. 35, no. Part 2, No. 1B, pp. L126–L129, Jan. 1996.
- [3] H. Masuda, F. Hasegawa, and S. Ono, “Self-Ordering of Cell Arrangement of Anodic Porous Alumina Formed in Sulfuric Acid Solution,” *J. Electrochem. Soc.*, vol. 144, no. 5, pp. L127–L130, May 1997.
- [4] H. Masuda, K. Yasui, and K. Nishio, “Fabrication of Ordered Arrays of Multiple Nanodots Using Anodic Porous Alumina as an Evaporation Mask,” *Adv. Mater.*, vol. 12, no. 14, pp. 1031–1033, Jul. 2000.
- [5] E. Y. Tsybal, A. Sokolov, I. F. Sabirianov, and B. Doudin, “Resonant Inversion of Tunneling Magnetoresistance,” *Phys. Rev. Lett.*, vol. 90, no. 18, p. 186602, May 2003.
- [6] S. Pramanik, S. Bandyopadhyay, and M. Cahay, “Spin relaxation in the channel of a spin field-effect transistor,” *IEEE Trans. Nanotechnol.*, vol. 4, no. 1, pp. 2–7, Jan. 2005.
- [7] R. C. Furneaux, W. R. Rigby, and A. P. Davidson, “The formation of controlled-porosity membranes from anodically oxidized aluminium,” *Nature*, vol. 337, no. 6203, pp. 147–149, Jan. 1989.
- [8] S. Bandyopadhyay, A. E. Miller, H. C. Chang, G. Banerjee, V. Yuzhakov, D.-F. Yue, R. E. Ricker, S. Jones, J. A. Eastman, E. Baugher, and M. Chandrasekhar, “Electrochemically

- assembled quasi-periodic quantum dot arrays,” *Nanotechnology*, vol. 7, no. 4, p. 360, Dec. 1996.
- [9] X. Zhang, Y. Hao, G. Meng, and L. Zhang, “Fabrication of Highly Ordered InSb Nanowire Arrays by Electrodeposition in Porous Anodic Alumina Membranes,” *J. Electrochem. Soc.*, vol. 152, no. 10, pp. C664–C668, Oct. 2005.
- [10] H. Zeng, M. Zheng, R. Skomski, D. J. Sellmyer, Y. Liu, L. Menon, and S. Bandyopadhyay, “Magnetic properties of self-assembled Co nanowires of varying length and diameter,” *J. Appl. Phys.*, vol. 87, no. 9, pp. 4718–4720, May 2000.
- [11] M. Zheng, L. Menon, H. Zeng, Y. Liu, S. Bandyopadhyay, R. D. Kirby, and D. J. Sellmyer, “Magnetic properties of Ni nanowires in self-assembled arrays,” *Phys. Rev. B*, vol. 62, no. 18, pp. 12282–12286, Nov. 2000.
- [12] R. H. Geiss and J. Silcox, “Effect of Dislocation Distribution on the Coercivity of Nickel Single Crystals,” *J. Appl. Phys.*, vol. 39, no. 2, pp. 982–983, Feb. 1968.
- [13] S. Pramanik, C.-G. Stefanita, S. Patibandla, S. Bandyopadhyay, K. Garre, N. Harth, and M. Cahay, “Observation of extremely long spin relaxation times in an organic nanowire spin valve,” *Nat. Nanotechnol.*, vol. 2, no. 4, pp. 216–219, Apr. 2007.
- [14] V. K. Arora and M. Jaafarian, “Effect of nonparabolicity on Ohmic magnetoresistance in semiconductors,” *Phys. Rev. B*, vol. 13, no. 10, pp. 4457–4461, May 1976.
- [15] F. J. Jedema, M. V. Costache, H. B. Heersche, J. J. A. Baselmans, and B. J. van Wees, “Electrical detection of spin accumulation and spin precession at room temperature in metallic spin valves,” *Appl. Phys. Lett.*, vol. 81, no. 27, pp. 5162–5164, Dec. 2002.
- [16] Y. Takamura and S. Sugahara, “Analysis and control of the Hanle effect in metal–oxide–semiconductor inversion channels,” *J. Appl. Phys.*, vol. 111, no. 7, p. 07C323, Apr. 2012.

- [17] I. Appelbaum, B. Huang, and D. J. Monsma, “Electronic measurement and control of spin transport in silicon,” *Nature*, vol. 447, no. 7142, pp. 295–298, May 2007.
- [18] Y. Fukuma, L. Wang, H. Idzuchi, S. Takahashi, S. Maekawa, and Y. Otani, “Giant enhancement of spin accumulation and long-distance spin precession in metallic lateral spin valves,” *Nat. Mater.*, vol. 10, no. 7, pp. 527–531, Jul. 2011.
- [19] Z. H. Xiong, D. Wu, Z. Vally Vardeny, and J. Shi, “Giant magnetoresistance in organic spin-valves,” *Nature*, vol. 427, no. 6977, pp. 821–824, Feb. 2004.
- [20] S. Bandyopadhyay, M. I. Hossain, H. Ahmad, J. Atulasimha, and S. Bandyopadhyay, “Coherent Spin Transport and Suppression of Spin Relaxation in InSb Nanowires with Single Subband Occupancy at Room Temperature,” *Small*, vol. 10, no. 21, pp. 4379–4385, Nov. 2014.
- [21] N. Telang and S. Bandyopadhyay, “Effects of a magnetic field on electron-phonon scattering in quantum wires,” *Phys. Rev. B*, vol. 48, no. 24, pp. 18002–18009, Dec. 1993.
- [22] H. A. Nilsson, P. Caroff, C. Thelander, M. Larsson, J. B. Wagner, L.-E. Wernersson, L. Samuelson, and H. Q. Xu, “Giant, Level-Dependent g Factors in InSb Nanowire Quantum Dots,” *Nano Lett.*, vol. 9, no. 9, pp. 3151–3156, Sep. 2009.
- [23] K. L. Litvinenko, L. Nikzad, J. Allam, B. N. Murdin, C. R. Pidgeon, J. J. Harris, T. Zhang, and L. F. Cohen, “Spin lifetime in high quality InSb epitaxial layers grown on GaAs,” *J. Appl. Phys.*, vol. 101, no. 8, p. 83105, Apr. 2007.
- [24] P. Murzyn, C. R. Pidgeon, P. J. Phillips, J.-P. Wells, N. T. Gordon, T. Ashley, J. H. Jefferson, T. M. Burke, J. Giess, M. Merrick, B. N. Murdin, and C. D. Maxey, “Electron spin lifetimes in Hg<sub>0.78</sub>Cd<sub>0.22</sub> Te and InSb,” *Phys. E Low-Dimens. Syst. Nanostructures*, vol. 20, no. 3–4, pp. 220–223, Jan. 2004.

- [25] J. T. Olesberg, W. H. Lau, M. E. Flatté, C. Yu, E. Altunkaya, E. M. Shaw, T. C. Hasenberg, and T. F. Boggess, “Interface contributions to spin relaxation in a short-period InAs/GaSb superlattice,” *Phys. Rev. B*, vol. 64, no. 20, p. 201301, Oct. 2001.
- [26] S. M. Sze, *Physics of Semiconductor Device*. .
- [27] R. J. Elliott, “Theory of the Effect of Spin-Orbit Coupling on Magnetic Resonance in Some Semiconductors,” *Phys. Rev.*, vol. 96, no. 2, pp. 266–279, Oct. 1954.
- [28] P. C. Sercel and K. J. Vahala, “Polarization dependence of optical absorption and emission in quantum wires,” *Phys. Rev. B*, vol. 44, no. 11, pp. 5681–5691, Sep. 1991.
- [29] P. S. A. Kumar and J. C. Lodder, “The spin-valve transistor,” *J. Phys. Appl. Phys.*, vol. 33, no. 22, p. 2911, 2000.
- [30] M. I. Hossain, S. Bandyopadhyay, J. Atulasimha, and S. Bandyopadhyay, “Modulating spin relaxation in nanowires with infrared light at room temperature,” *Nanotechnology*, vol. 26, no. 28, p. 281001, Jul. 2015.
- [31] M. Julliere, “Tunneling between ferromagnetic films,” *Phys. Lett. A*, vol. 54, no. 3, pp. 225–226, Sep. 1975.
- [32] S. O. Valenzuela and M. Tinkham, “Spin-polarized tunneling in room-temperature mesoscopic spin valves,” *Appl. Phys. Lett.*, vol. 85, no. 24, pp. 5914–5916, Dec. 2004.
- [33] E. Y. Tsybal, O. N. Mryasov, and P. R. LeClair, “Spin-dependent tunnelling in magnetic tunnel junctions,” *J. Phys. Condens. Matter*, vol. 15, no. 4, p. R109, Feb. 2003.
- [34] E. O. Omayio, P. M. Karimi, W. K. Njoroge, and F. K. Mugwanga, “Current-voltage characteristics of p-CuO/n-ZnO: Sn Solar cell,” *Int J Thin Film Sci Tec*, vol. 2, no. 1, pp. 25–28, 2013.

- [35] M. I. Hossain, J. Edwards, J. Tyler, J. Anderson, and S. Bandyopadhyay, “Antimicrobial properties of nanorods: Chemical or physical kill?,” in *2015 IEEE Nanotechnology Materials and Devices Conference (NMDC)*, 2015, pp. 1–5.
- [36] M. I. Hossain, J. Atulasimha, and S. Bandyopadhyay, “Raman spectroscopy studies of phonons in a nanowire subjected to a magnetic field,” in *2015 IEEE Nanotechnology Materials and Devices Conference (NMDC)*, 2015, pp. 1–3.
- [37] D. Xu, A. Subramanian, L. X. Dong, and B. J. Nelson, “Shaping electrodes for ultrahigh precision dielectrophoretic manipulation of carbon nanotubes,” in *2008 IEEE/RSJ International Conference on Intelligent Robots and Systems*, 2008, pp. 8–13.
- [38] B. R. Burg, V. Bianco, J. Schneider, and D. Poulikakos, “Electrokinetic framework of dielectrophoretic deposition devices,” *J. Appl. Phys.*, vol. 107, no. 12, p. 124308, Jun. 2010.
- [39] N. K. R. Palapati, E. Pomerantseva, and A. Subramanian, “Single nanowire manipulation within dielectrophoretic force fields in the sub-crossover frequency regime,” *Nanoscale*, vol. 7, no. 7, pp. 3109–3116, Feb. 2015.
- [40] O. Song and Y. Maeda, “Magnetoresistance and Strain in Permalloy Films,” *J. Magn.*, vol. 3, no. 1, pp. 36–38, 1998.

# Curriculum Vitae

Md Iftekhar Hossain

Date of birth: 16 th September, 1988

Nationality: Bangladesh

Email: hossaini@vcu.edu, mithun.iftekhar@gmail.com

## **EDUCATION:**

- **PhD**, Electrical and Computer Engineering, May 2016, Virginia Commonwealth University (VCU), Richmond, VA. **GPA-4.00/4.00**  
**Dissertation Title:** Coherent spin transport in nanowire spin valves and novel spintronic device possibilities
- **B.S.**, Electrical and Electronic Engineering, Feb. 2011, Bangladesh Uni. of Eng. & Tech (BUET), Dhaka, BD. **GPA: 3.75/4.0**

## **Research and Professional Experience:**

**Graduate Research assistant**, Quantum Device Lab., Virginia Commonwealth University, August 2012-May 2016.

**Software Engineer**, Samsung Bangladesh R&D Center, March 2011- July 2012.

## **Major Publications:**

### **Journal:**

1. **M.I.Hossain**, S.Bandyopadhyay, J. Atulasimha, S. Bandyopadhyay “Modulation of D’yakonov-Perel’ spin relaxation in InSb nanowires with infrared illumination at room temperature”, *Nanotechnology*, 26, 281001 (2015). **Featured in** Nanotechweb.org
2. S. Bandyopadhyay, **M.I. Hossain**, H. Ahmad, J. Atulasimha, S. Bandyopadhyay “Coherent Spin Transport and Suppression of Spin Relaxation in InSb Nanowires with Single Subband Occupancy at Room Temperature”, *Small*, 10, 4379 (2014).
3. S Sayed, **M.I .Hossain**, M.Z.R. Khan” A subthreshold swing model for thin-film fully depleted SOI four-gate transistors” *Electron Devices, IEEE Transactions on* 59 (3), 854-85
4. **M.I.Hossain**, M.Maksud, N.K.R. Palapati, A. Subramanian, J. Atulasimha, S. Bandyopadhyay “Super-giant magnetoresistance in copper nanowires due to magnetic field modulation of potential barrier heights at nanowire-contact interfaces”submitted to APL.

5. **M.I.Hossain**, M.Maksud, N.K.R. Palapati, A. Subramanian, J. Atulasimha, S. Bandyopadhyay “Anisotropic magnetoresistance(AMR) in a single nanowire system and how it can be effected by the strain” in progress

**Conference:**

1. **Md. I. Hossain**, J. Atulasimha, and S. Bandyopadhyay, “Raman spectroscopy studies of phonons in a nanowire subjected to a magnetic field” in Submitted to IEEE Nanotechnology Materials and Devices Conference, Anchorage, Alaska, 2015.

2. **Md. I. Hossain**, J. Edwards, J. Tyler, J. Anderson and S. Bandyopadhyay “Antimicrobial Properties of Nanorods: Chemical or Physical Kill?” in IEEE Nanotechnology Materials and Devices Conference, Anchorage, Alaska, 2015

3. S. Sayed, **M. I. Hossain**, R. Huq, and M. Z. R. Khan, "Three Dimensional Modeling of SOI Four Gate Transistors" in Nanotechnology Materials and Devices Conference. Proceedings. 2010 IEEE, Monterey, California, USA, 2010, pp. 383-388.

4. S. Sayed, **M. I. Hossain**, R. Huq, and M. Z. R. Khan, "Analytical Expression of the Three-Dimensional Potential Distribution of a SOI Four-Gate Transistor" in International Conference on Electrical & Computer Engineering (ICECE), 2010.

5. E. M. A. Anas, **M. I. Hossain**, M. S. Afran and S. Sayed "Compression of ECG signals exploiting correlation between ECG” in International Conference on Electrical & Computer Engineering (ICECE), 2010.

**Poster and Oral Presentation:**

1. Poster presentation of “Coherent Spin Transport in Nanowire Spin Valves and Novel Spintronic Device Possibilities” at Graduate Research Symposium, VCU-2015.

2. Poster presentation of “Modulating D’yakonov-Perel’ Spin Relaxation In Single Moded Quantum Wires With Light” at International Symposium on Cluster and Nanomaterials, Richmond, VA, 2015.

3. Poster and oral presentation of “Three-Dimensional Analytical Modeling of SOI Four Gate Transistors (G<sup>4</sup>-FET).” at EEE undergraduate project workshop EUPROW, Bangladesh University of Engineering and Technology Dhaka, Bangladesh, March 12, 2011

4. Poster presentation of “The Antimicrobial Properties of Silver Nanostructures” at DERI 2014-2015

5. Oral Presentation of “Raman spectroscopy studies of phonons in a nanowire subjected to a magnetic field” at IEEE NMDC Conference, Anchorage (AK), 2015.

6. Oral Presentation of “Antimicrobial Properties of Nanorods: Chemical or Physical Kill?” at IEEE NMDC Conference, Anchorage (AK), 2015.

### **Awards and Honors:**

- Received runner up award as “Outstanding Graduate Research Assistant” from ECE department at VCU in May 2016.
- Received Graduate Student Travel Grant from ECE department to attend APS March Meeting, 2016.
- Received “DERI-travel grant” to attend the “ISCAN-2015” conference in 2015.
- Level-1 (2007) & Level-2(2008) Deans’ list Scholarship in BUET.
- HSC(Higher Secondary Certificate) board scholarship from Chittagong Board, 2005.
- 4<sup>th</sup> position in annual science fair in Ispahani Public School and College, Chittagong. (2004)
- 2nd Runner Up in Dutch Bangla math Olympiad, Chittagong, Bangladesh (2004)
- Junior Scholarship award from Chittagong Board, 2000.

### **Activities and Membership:**

- Mentoring in the DURi (2016), DERi (2014-2015) and RAPME (2013, 2014, 2015) Program at Virginia Commonwealth University.
- Served as the Webmaster in Engineering Graduate Students Association @VCU (2014-2015)
- Served as the President of Bangladeshi Students’ Organization @ VCU (2014-2015).
- Student member of American Physical Society (APS)
- Student member of IEEE, \_IEEE Nanotechnology Council, \_IEEE Electron Devices Society, IEEE Magnetics Society
- Member of The Institution of Engineers Bangladesh (IEB Chittagong Center)